Physics – Uspekhi **58** (1) 33 – 60 (2015)

REVIEWS OF TOPICAL PROBLEMS

PACS numbers: 61.43.Hv, 61.46.Df, 62.20.de, 62.23.Pq

Structure and properties of particulate-filled polymer nanocomposites

G V Kozlov

DOI: 10.3367/UFNe.0185.201501c.0035

Contents

Abstract. **Some properties of particulate-filled polymer nanocomposites, including structural features, are reviewed. Novel effects found in these materials, such as nanoadhesion and reinforcement mechanisms, are discussed. A structural analysis is performed using a fractal analysis procedure and the cluster model of the structure of a polymer in an amorphous state. The application prospects of these materials are examined in comparison with other polymer nanocomposites.**

Keywords: polymer, nanocomposite, disperse nanoparticles, structure, aggregation, interfacial adhesion, nanoadhesion, fractal analysis, percolation, reinforcement degree, yielding, failure, microhardness

1. Introduction

At present, polymer nanocomposites are considered to be one of the most promising structural materials [1]. There are three main classes of these nanomaterials, viz. particulate-filled polymer nanocomposites, polymer/organoclays, and polymer/carbon nanotubes (nanofibers). Despite the similarity of the basic principles to describe them, the structural features of these nanofillers in a polymeric matrix are essentially different and should be taken into consideration in any detailed description of concrete nanocomposites, especially in the case of aggregation of nanofiller particles. This makes it impossible to define the difference between particulate-filled nanocomposites and nanocomposites with anisometric particles. For all that, the three aforementioned classes of polymer nanocomposites do differ, which in the most general physical terms lies in the dimensionality of nanofiller particles. This factor necessitates an individual description of each class of polymer nanocomposites.

Thus far, the emphasis has been placed on nanocomposites filled with layered silicates (organoclays) [2–6] or nanotubes (nanofibers) [7–10], whereas particulate-filled polymer nanocomposites have attracted much less attention. However, the potential of the latter class of polymer materials is far from exhausted [5, 6, 11–17]. To begin with, methods for their analysis are poorly developed, despite a very large number of their known species and a wide variety of industrial applications. This is the main factor restricting the possibility of predicting the limiting characteristics of such materials [1, 7–11].

The present review is designed to describe certain specific structural features and properties of this class of polymer nanocomposites that have been given insufficient attention, despite their theoretical and practical importance. Also considered in the review are prospects for the application of particulate-filled polymer nanocomposites in comparison with other classes of analogous materials.

2. Structural features of particulate-filled polymer nanocomposites

2.1 Nanoadhesion effect

The leading role in the formation of properties of multiphase materials is played by the level of interfacial interaction [18], which fully applies to polymer composites (nanocomposites). The authors of Ref. [19] have demonstrated that a rise in the filler content of polymer composites with well apparent interfacial adhesion increases the modulus of elasticity, whereas the absence of interfacial adhesion in the polymer matrix–filler structure leads to its decrease. However, determination of the adhesion level in polymer composites

---

G V Kozlov Berbekov Kabardino-Balkarian State University,
ul. Chernyshevskogo 173, 360004 Nal'chik, Kabardino-Balkarian Republic, Russian Federation
Tel. +7 (866) 242 41 44. Fax +7 (495) 337 99 55
E-mail: i_dolbin@mail.ru

Received 21 April 2013, revised 16 June 2014
Uspekhi Fizicheskikh Nauk **185** (1) 35 – 64 (2015)
DOI: 10.3367/UFNr.0185.201501c.0035
Translated by Yu V Morozov; edited by A Radzig

by experimental methods encounters some difficulties. For example, adhesion strength measured by standard methods may be significantly different due to a number of overlooked effects in real composites, such as aggregation of filler particles [20–22], changes in the polymer matrix structure caused by introduction of the filler [23–26], and some other factors. Interfacial phenomena influence practically all properties of polymer composites. As a practical matter, therefore, an evaluation of interfacial adhesion from the macroscopic properties of a composite by the available methods (see, e.g., Refs [27–31]) appears to be the most convenient method for the determination of this parameter in bulk composites. The authors of Refs [32–35] determined the level of interfacial adhesion and factors affecting it in particulate-filled phenylone/aerosyl nanocomposites based on observations of their thermal expansion.

An isophthalic acid-based linear heterochain homopolymer and phenylone C-2 (aromatic amorphous polyamide) were used as polymeric binders for the nanocomposites being considered, whereas aerosyl with a mean particle diameter of 25 nm and a specific surface of 300 $\mathrm{m^2\,g^{-1}}$ served as a disperse nanofiller. The nanofiller was introduced into the polymer matrix in a rotating electromagnetic field with the aid of nonequiaxial ferromagnetic particles with the length-to-diameter ratio of 4–5. The volume of these particles charged into the reactor was 0.04–0.05 of the field action volume; electromagnetic induction of this field varied from 0.08 to 0.12 T. Under these experimental conditions, the optimal time of nanocomposite treatment in the electromagnetic field ranged within 270–300 s.

The treatment of powdered phenylone/aerosyl composites in the rotating magnetic field (MF) allows aggregation of nanofiller particles to be suppressed (or reduced). To verify the realization of this effect, the specimens of phenylone/aerosyl composites were prepared by simple mechanical mixing of the two constituents. In what follows, samples of such nanocomposites obtained in the rotating electromagnetic field are designated phenylone/aerosyl-MF, and those prepared by mechanical mixing are referred to as phenylone/aerosyl.

The solid lines *1–3* in Fig. 1 illustrate three main types of the dependence of linear thermal expansion coefficients of the nanocomposites of interest, α_c, on the nanofiller volumetric filling degree φ_n. The straight line *1* shows the case of the absence of adhesion between two phases of the nanocomposite, as $\alpha_m > \alpha_n$ (α_m, α_n are thermal expansion coefficients of the polymer matrix and the nanofiller, respectively); this inequality is always fulfilled for inorganic fillers (nanofillers) [36]. In the absence of permanent compressive strain, the polymeric matrix expands upon heating regardless of the nature of nanofiller particles; in such a case, $\alpha_c = \alpha_m$ [36]. Straight line *2* corresponds to the simple mixture rule [36]:

$$\alpha_c^{\mathrm{mix}} = \alpha_m (1 - \varphi_n) + \alpha_n \varphi_n \,, \tag{1}$$

where α_c^{mix} is the thermal expansion coefficient of the mixture.

Rule (1) holds only for an ideal case when each phase expands independently of the other. Finally, curve *3* corresponds to the Turner equation [36]

$$\alpha_c^{\mathrm{T}} = \frac{\alpha_m (1 - \varphi_n) K_m + \alpha_n \varphi_n K_n}{(1 - \varphi_n) K_m + \varphi_n K_n} \,, \tag{2}$$

where K_m and K_n are the bulk moduli of the polymer matrix and the nanofiller, respectively.

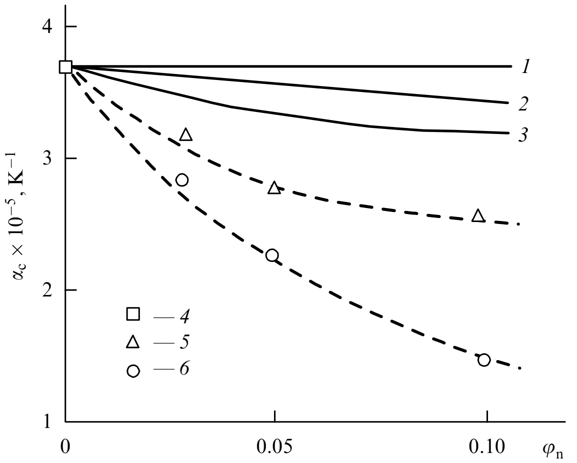

Figure 1. Dependence of linear thermal expansion coefficient α_c on nanofiller volumetric filling degree φ_n. *1* — the absence of interfacial adhesion, *2* — the mixture rule, *3* — Turner's equation, *4–6* — experimental data for phenylone (4), phenylone/aerosyl (5), and phenylone/aerosyl-MF (6) [33].

Formula (2) was derived by P S Turner on the following assumptions: homogeneous composition, the absence of residual stress across the entire volume, identical relative deformation in the matrix and the filler, and the absence of shear strains. A disadvantage of this formula is that it was obtained on the assumption that the thermal expansion coefficient depends on the filler volume fraction alone. Clearly, this assumption is in conflict with experimental data: both the size and the shape of the filler particles exert an appreciable influence on the effective thermal expansion coefficient of the composite. This disadvantage can be neglected for an isotropic filler and a small variation of its size. The remaining assumptions are met to a certain degree for each real composite (nanocomposite), the criterion for validity of the theoretical formula being its agreement with experiment that is close enough for the Turner equation [36].

The points in Fig. 1 denote experimental α_c values, including those for phenylone ($\alpha_c = \alpha_m$). Notice that the Turner equation contained the values of Young's modulus E instead of the bulk modulus K. As is known [36], such a substitution permits determining the lower bound of quantity α_c for polymer composites. It follows from Fig. 1 that the values of α_c for both series of aerosyl-filled nanocomposites lie much below the curve calculated from Turner's equation, i.e., they are significantly smaller than the lower limiting α_c values for polymer composites. Moreover, α_c for phenylone/aerosyl-MF nanocomposites are much lower than the respective values for phenylone/aerosyl nanocomposites. In other words, suppression (or reduction) of aerosyl particle aggregation markedly decreases α_c.

Let us consider the physical basis of the above changes in α_c for phenylone/aerosyl nanocomposites. The interaction between the polymer matrix and the filler (the interfacial adhesion level) can be evaluated using parameter b_α found from equation [36]:

$$\alpha_c = \alpha_c^{\mathrm{mix}} - b_\alpha (\alpha_c^{\mathrm{mix}} - \alpha_c^{\mathrm{T}}) \,. \tag{3}$$

The greater parameter b_α, the greater the interfacial adhesion level. For a large enough number of polymer composites with different matrices and fillers, b_α varies from

-0.19 to 1.39 [36]. The calculations from Eqn (3) for the nanocomposites being considered showed that $b_\alpha \approx 12$ for phenylone/aerosyl-MF, $b_\alpha \approx 6$ for phenylone/aerosyl, and b_α varies from ~ 5.40 to 0.35 for phenylone/silicon–yttrium oxynitride (SYON), decreasing with increasing φ_n (Fig. 2) [32]. In other words, the level of polymer matrix–nanofiller interaction in these nanocomposites may be significantly higher (by an order of magnitude) than in microcomposites. Following Ref. [37], the authors of Refs [32–35] called this effect nanoadhesion. To recall, Ref. [37] reports measurement of adhesion in two-layer polystyrene films at the micro- and nanolevels. It turned out that the adhesion strength in the latter case was considerably higher than in the former. The authors of Ref. [37] attributed this effect to the difference in the degree of completion for the formation of the interface layer between the two polystyrene films.

The cause of nanoadhesion in nanocomposites lies in the small value of contact area between the polymer matrix and the nanofiller. The small contact area between an individual particle of the nanofiller and the polymer matrix suggests a large contact area per unit volume of a nanocomposite due to its multiple interfaces [38], as confirmed by numerous observations. It has recently been revealed [17] that the thickness of the intermediate (interfacial) layer in polymer/carbon nanotube nanocomposites varies within ~ 125–225 nm, i.e., by an order of magnitude greater than the nanotube diameter proper. Notice that the interfacial adhesion level in nanocomposites is controlled by two factors: (1) the number of contacts between the polymer matrix and the nanofiller particle (particle aggregate) surface, and (2) the strength of physical and/or chemical interactions between these constituents.

The first of these factors is actually related to the aforementioned multiple interfaces in nanocomposites. In what follows, it will be shown that the adhesion effect is only manifested when the size of disperse particles is below 80 nm, i.e., only in the case of nanoparticles. It follows from the comparison of aerosyl and SYON particles (mean diameter 64 nm) and the data of Fig. 2 that the value of b_α depends at least on two factors, namely, the size of filler particles and the degree of their aggregation, i.e., the size of nanoaggregates in the end. The value of b_α for aerosyl is higher than for silicon–yttrium oxynitride (particle sizes 25 and 64 nm, respectively). For phenylone/aerosyl-MF nanocomposites, b_α is twice that for phenylone/aerosyl nanocomposites, because an aggregation level of aerosyl particles decreases when the powdered phenylone/aerosyl mixture is treated in a rotating electromagnetic field (see above). Moreover, the decrease in b_α with increasing φ_n for phenylone/SYON nanocomposites (see Fig. 2) is also due to the enhancement of aggregation of silicon–yttrium oxynitride particles with the growth of their content.

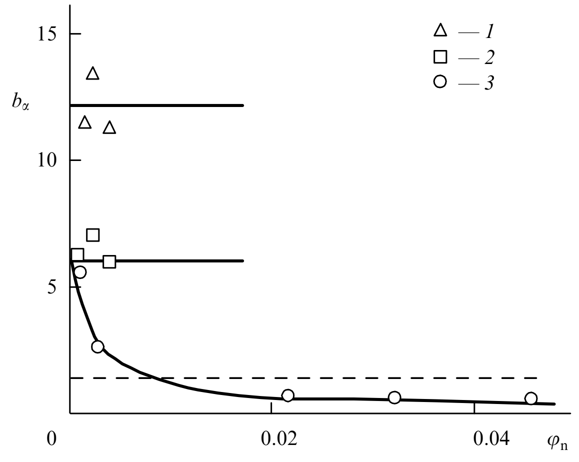

Figure 2. Dependences of parameter b_α on nanofiller volumetric filling degree φ_n for phenylone/aerosyl-MF (*1*), phenylone/aerosyl (*2*), and phenylone/SYON (*3*) nanocomposites. Horizontal dashed line indicates the upper limiting value b_α for microcomposites [32].

Micrographs of the surface of phenylone/aerosyl (Fig. 3a–c) and phenylone/aerosyl-MF (Fig. 3d–f) samples containing 1 mass % aerosyl, which were obtained with the use of a Zygo New View 5022 surface structure analyzer, demonstrate suppression of aggregation in the latter series of nanocomposites. Figure 3d is especially remarkable in this context, since it shows up a 'cloud' of aerosyl particles that failed to aggregate after their preliminary treatment in the electromagnetic field. In contrast, the micrographs in Fig. 3a–c show the well apparent aggregation of aerosyl particles into sufficiently large structures.

These data confirm the earlier conclusion that the observed nanoadhesion effect is a purely dimensional or true nanoeffect [38]. As is well known, it is impossible to achieve perfect contact between the surfaces of a pair of different materials when measuring the adhesion strength. Such contact is only realized through certain surface protrusions, which accounts for the small contact area and decreases the adhesion strength [39]. Large protrusions and depressions are hardly possible on the rather small (nanoscale) contact area, which accounts for a sharp rise in the adhesion level. This condition can be expressed more specifically: nanoadhesion shows its worth when the participants, i.e., nanoparticles and a macromolecular coil, are of the same scale [34].

The dependence of parameter b_α on the mean surface area S_p of nanofiller particles (shaped like spheres) for phenylone/aerosyl-MF, phenylone/aerosyl, and phenylone/SYON nanocomposites is illustrated in Fig. 4. Clearly, b_α or the interfacial adhesion level decrease as S_p (the size of filler nanoparticles) increases; at $S_p \approx 2 \times 10^4$ nm^2, corresponding to a particle diameter of ~ 80 nm, this dependence asymptotically tends to $b_\alpha \approx 1$, i.e., to perfect microadhesion ($\alpha_c = \alpha_c^T$), as follows from Eqn (3).

The nanoadhesion effect strongly affects the macroscopic properties of polymer nanocomposites. It follows from Fig. 1 that the introduction of 1 mass % of aerosyl into phenylone results in a roughly threefold decrease in α_c (for phenylone/aerosyl-MF nanocomposites). For a similar decrease in α_c in microcomposites, the filler volume fraction must be $\varphi_n = 0.3 - 0.7$ [36], i.e., almost two orders of magnitude higher. A twofold decrease in α_c in polyamide-6/Na$^+$-montmorillonite nanocomposites is reached by introducing 4.7 mass % of organoclay [40]. A comparative analysis of the influence of nanoadhesion on the mechanical and thermal properties of nanocomposites will be presented in respective Sections 3 and 4 below.

To sum up, the above data demonstrate the nanoadhesion effect in particulate-filled polymer nanocomposites in the form of a markedly enhanced polymer matrix–nanofiller interaction. This effect is of a purely dimensional nature, being realized for filler nanoparticles less than 80 nm in diameter. The nanoadhesion effect exerts a strong influence on the macroscopic properties of those nanocomposites in which it occurs [32–35].

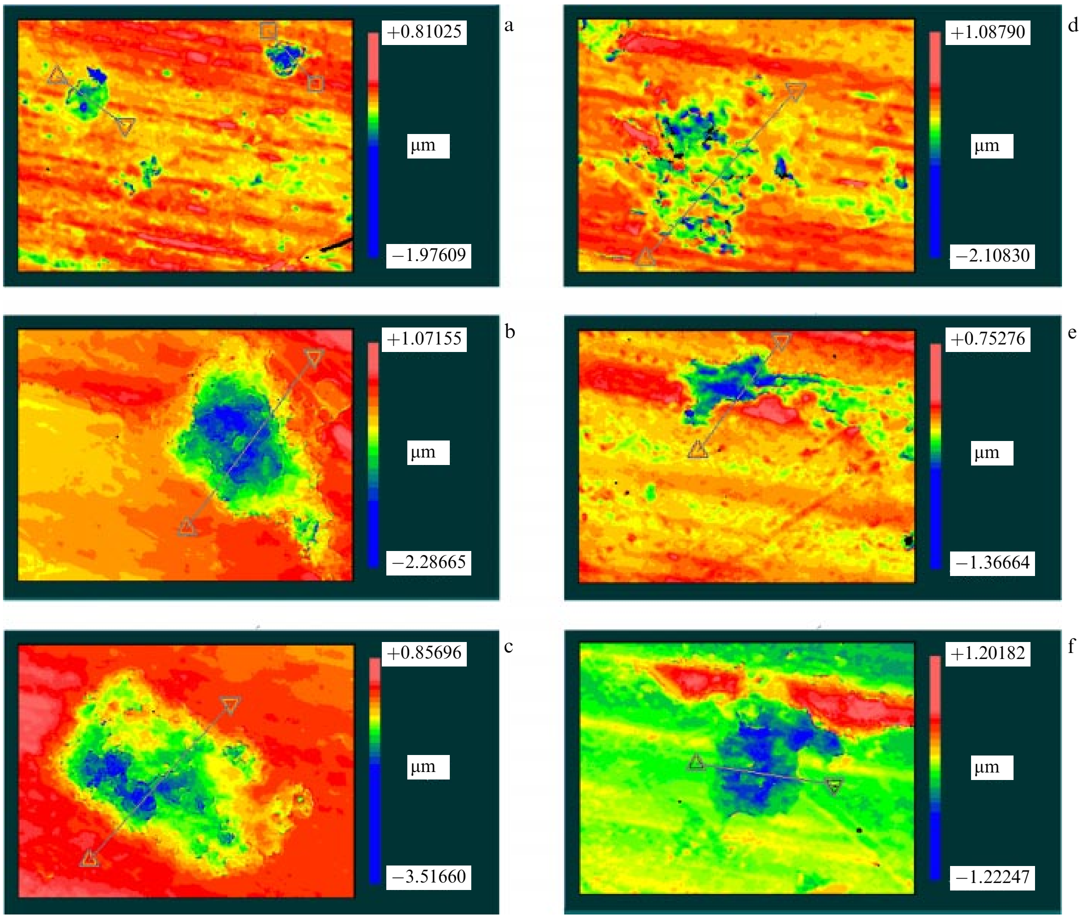

Figure 3. Electron micrographs of phenylone/aerosyl (a–c) and phenylone/aerosyl-MF (d–f) nanocomposite surfaces [33].

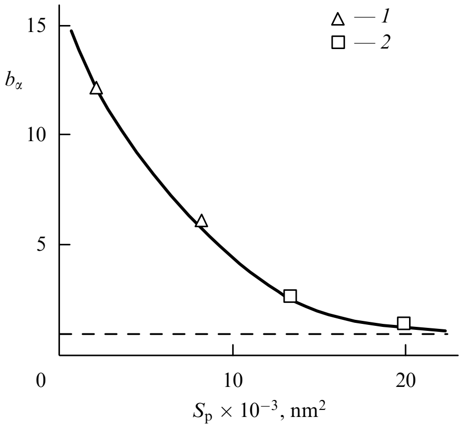

Figure 4. Dependence of parameter b_α on the mean surface area S_p of nanofiller particles for nanocomposites filled with aerosyl (*1*) and silicon-yttrium oxynitride (*2*). Horizontal dashed line indicates the perfect microadhesion level ($b_\alpha = 1$) [34].

2.2 Theoretical description of nanoadhesion effect: fractal models

The authors of Ref. [41] undertook a theoretical study of the factors that are responsible for the nanoadhesion effect in particulate-filled polymer nanocomposites and determined its magnitude. It is known [29] that the polymer–filler interplay in polymer composites (nanocomposites) depends on two groups of factors: physical and/or chemical and structural ones. The surface of disperse particles of a nanofiller, with which the polymer matrix interacts, represents a fractal object [42, 43], which means that the number N_u of contact sites depends on the dimension of the nanoparticle surface d_u accessible (unshielded) for such a contact and is defined as [44, 45]

$$N_u \sim r_p^{d_u}\,, \tag{4}$$

where r_p is the radius of a nanofiller particle.

Dimension d_u, in turn, is related to fractal dimension d_s of the nanofiller particle surface and is governed by equation [38]

$$d_u = d_s - 1 + \frac{d - d_s}{d_w}\,, \tag{5}$$

where d is the dimension of an Euclidean space in which the fractal is considered (in our case, $d = 3$), and d_w is the dimension of a random walk on the fractal that can be estimated based on the Aharony–Stauffer argument [44]:

$$d_w = d_s + 1\,. \tag{6}$$

Dimension d_s is calculated from equation [46]

$$S_u = 410\left(\frac{D_p}{2}\right)^{d_s - d}, \tag{7}$$

where the particle specific surface S_u is given in m^2 g^{-1}, and the particle's diameter D_p in nm.

It was shown for $d_u > 1.50$ [47] that the effective quantity d_u^{eff} of this dimension decreases as its nominal value increases.

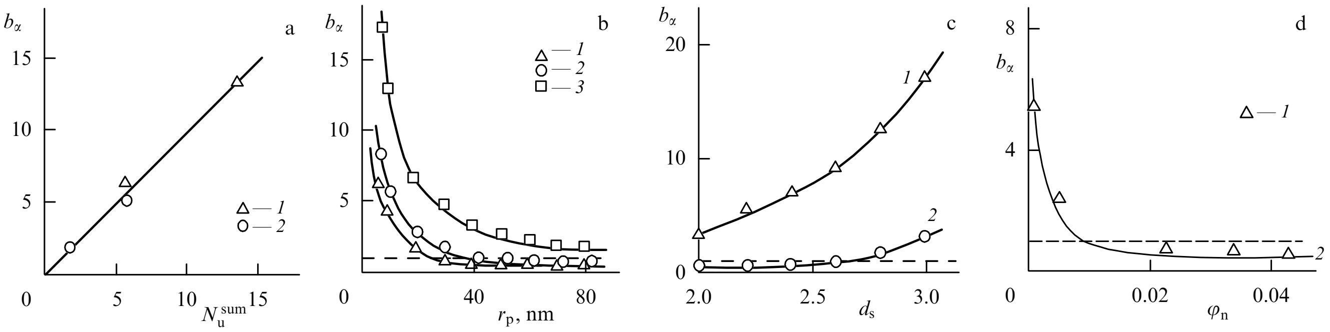

Figure 5. (a) Dependence of parameter b_α on the number N_u^{sum} of unshielded contact sites on the nanofiller particle surface for phenylone/aerosyl (*1*) and phenylone/SYON (*2*) nanocomposites [41]. (b) Dependences of parameter b_α on radius r_p of nanofiller particles having surface dimension $d_s = 2.0$ (*1*), 2.5 (*2*), and 3.0 (*3*). Horizontal dashed line in Figs 5 b–d indicates the level of perfect microadhesion ($b_\alpha = 1$) [41]. (c) Dependences of parameter b_α on the surface dimension d_s of nanofiller particles having radius $r_p = 20$ (*1*) and 40 (*2*) nm [41]. (d) Dependences of parameter b_α on nanofiller volume fraction φ_n for phenylone/SYON nanocomposites, obtained in experiment (*1*) and calculated from Eqns (11) and (12) (*2*) [41].

The observed behavior is described by the following equation

$$d_u^{eff} = 2 - d_u \,. \tag{8}$$

Relation (4), with the substitution of d_u^{eff} for d_u, is obtained for a single nanofiller particle, while the number of such particles per nanocomposite unit volume can be calculated as [48]

$$N_p = \frac{\varphi_n}{V_p} \,, \tag{9}$$

where V_p is the particle's volume found from its diameter D_p on the assumption of the spherical shape of such particles.

Taking $\varphi_n = \text{const}$ yields the equation for the calculation of the total number of contact sites between the polymer matrix and the nanofiller, N_u^{sum} ($N_u^{sum} = N_u N_p$) [48]:

$$N_u^{sum} = \frac{c_{pc}}{r_p^{3-d_u}} \,, \tag{10}$$

where the constant c_{pc} is introduced because relation (4) contains a proportionality sign that by its meaning is an indicator of the level of physical and/or chemical interactions between the polymeric matrix and the nanofiller [29]. Evidently, this constant is different for various polymer matrix–nanofiller combinations. From this point on, the quantity c_{pc} will be chosen to be constant for a fixed polymer matrix–nanofiller pair in order to satisfy the following approximate condition [5]:

$$b_\alpha \approx N_u^{sum} \,, \tag{11}$$

because the last parameter is given in arbitrary units on account of the method used to calculate it.

Calculations utilizing Eqn (10) showed that, with such a choice of constant c_{pc}, parameters b_α and N_u^{sum} are roughly equal for both series of nanocomposites being considered, but different constants c_{pc} for phenylone/aerosyl and phenylone/SYON nanocomposites (317 and 882, respectively) are needed to arrive at the common linear relationship $b_\alpha(N_u^{sum})$ in Eqn (10). This points to the fact that the level of physical and/or chemical phenylone–SYON interactions is three times that of phenylone — aerosyl interactions. The dependence $b_\alpha(N_u^{sum})$ for the nanocomposites of interest proved linear and passed through the origin of coordinates (Fig. 5a). This condition is needed to ensure that the above correlation is correct: it is understandable that interfacial adhesion cannot also be realized as a phenomenon ($b_\alpha = 0$) in the absence of polymer matrix–nanofiller contact sites or $N_u^{sum} = 0$ [6].

Importantly, the data of Fig. 5a suggest that the interfacial adhesion level for a phenylone–aerosyl pair is substantially higher than for a phenylone–SYON pair, despite the significantly higher c_{pc} value for the latter. This emphasizes the significance of structural factors determining the interfacial adhesion (nanoadhesion) level in polymer composites. Such a relationship between c_{pc} and structural factors follows from Eqn (10): if parameter b_α is directly proportional to c_{pc}, its dependence on r_p and d_u has a power-like, i.e., a stronger, form. The structural parameters include the size of nanofiller particles, characterized by their radius r_p, the nanofiller particle surface structure, characterized by dimension d_s, and the degree of nanofiller particle aggregation, characterized by aggregate radius R_{ag}. Let us consider the influence of these structural parameters.

Figure 5b displays the dependences of parameter b_α on the nanofiller particle radius in the range $r_p = 7.5-80$ nm at three fixed d_s dimensions: 2.0 (Euclidean surface), 2.5, and 3.0, which were calculated from Eqn (10) taking account of the condition $b_\alpha \approx N_u^{sum}$. As expected [32], the nanoadhesion effect can be realized only in the range of $r_p = 7.5-40$ nm, although this interval for particles with a very rough surface ($d_s = 3.0$) is somewhat wider even if at relatively low b_α values in a range of 2–3 [5].

Dependences $b_\alpha(d_s)$ calculated in a similar way for two fixed values of $r_p = 20$ and 40 nm (Fig. 5c) confirm in essence the conclusions drawn from the data of Fig. 5b. Indeed, a marked increase of b_α with increasing d_s occurs for small nanofiller particles with radius $r_p = 20$ nm, whereas a weak nanoadhesion effect can be realized at the limiting value of $r_p = 40$ nm only for large d_s ($d_s > 2.7$).

Reference [32] demonstrates the strong influence of SYON particle aggregation in phenylone/SYON nanocomposites as an example on the b_α value, apparent as its marked decrease with increasing φ_n (see Fig. 2). It was shown for polyhydroxyether/graphite polymer composites that aggregation of the filler particles obeys the following relationship [49]

$$R_{ag} \sim \varphi_n^{1/2} \,, \tag{12}$$

where R_{ag} and φ_{n} are the aggregate radius of graphite particles and their volume fraction, respectively.

Given that relationship (12) is equally correct for the description of SYON particle aggregation and the proportionality constant in this relationship is found from the condition $R_{\text{ag}} = 32$ nm at $\varphi_{\text{n}} = 0.0009$ (i.e., on the assumption that aggregation does not occur at the minimum φ_{n} value), it is possible to calculate the quantity $b_\alpha = N_{\text{u}}^{\text{sum}}$ from Eqn (10) at $c_{\text{pc}} = 882$ and compare it with the experimental data presented in Fig. 2 [32]. Such a comparison showed an excellent agreement between experiment and theory (calculated by the above method) (Fig. 5d). Worthy of note is the strong influence of aggregation on b_α apparent as a 14-fold decrease in b_α or the level of interfacial adhesion with a 50-fold increase in the silicon–yttrium oxynitride content, which results in approximately a seven-fold rise in R_{ag} compared with r_{p}.

Thus, the above results obtained by applying notions of fractal analysis indicate that the level of interfacial adhesion (nanoadhesion) in particulate-filled polymer nanocomposites depends on three factors, viz. the size of the filler particles, the degree of their aggregation, and the structure of their surfaces. As expected, the strongest influence on the realization of the nanoadhesion effect is exerted by the first two factors, because this effect is of dimensional origin [32–35]. Moreover, the level of physical and/or chemical interconstituent interaction has a certain effect on parameter b_α for different polymer–nanofiller pairs [41].

In Refs [50, 51], theoretical investigations into the nanoadhesion effect in particulate-filled polymer nanocomposites were conducted in the framework of the thermodynamic fractal approach [52]. The authors of Ref. [52] considered the thermodynamic model of sorption phenomena on fractal objects and showed that volume ϑ occupied by a fractal object with unit mass is defined by the equation

$$\vartheta = \rho_0^{-1} m_0^{1-3/d_{\text{s}}} \,, \tag{13}$$

where ρ_0 is the nanofiller density, and m_0 is the nanofiller particle mass. For polymer nanocomposites, the polymer layer adsorbed by a nanofiller particle can be regarded as the interfacial layer, and volume ϑ as the volume of the nanoparticle proper and the interfacial layer. In this case, the ratio between volume fractions of the interfacial layer (φ_{int}) and the nanofiller (φ_{n}) can be written in the form

$$\frac{\varphi_{\text{int}}}{\varphi_{\text{n}}} = \frac{\vartheta}{\vartheta_0} = \frac{m^{1-3/d_{\text{s}}}}{\rho m_0/\rho_0} \approx \frac{1}{m_0^{3/d_{\text{s}}}} \,, \tag{14}$$

where ρ is the polymer matrix density.

Let us consider methods for the evaluation of parameters entering in Eqn (14). The value of m_0 for an unaggregated nanofiller was estimated as the mass of a sphere of density ρ_0 [53]:

$$\rho_0 = 0.188 (D_{\text{p}})^{1/3} \quad [\text{kg m}^{-3}] \,. \tag{15}$$

Then, the relationship between φ_{int} and φ_{n} in thermodynamic interpretation can be written out as [50]

$$\varphi_{\text{int}} = k \varphi_{\text{n}} \,, \tag{16}$$

where

$$k = m_0^{-3/d_{\text{s}}} \,. \tag{17}$$

Another relationship between φ_{int} and φ_{n}, obtained in the framework of fractal analysis [33], has the form

$$\varphi_{\text{int}} = c \varphi_{\text{n}} b_\alpha \,, \tag{18}$$

where c is the coefficient of proportionality between φ_{int} and φ_{n} under the conditions of perfect microadhesion, i.e., at $b_\alpha = 1$. For phenylone-based nanocomposites filled with unaggregated aerosyl (phenylone/aerosyl-MF), aggregated aerosyl (phenylone/aerosyl), SYON, and β-sialon (a solid Al_2O_3 and AlN solution in β-Si_3N_4), the values of c are 1.08, 0.26, 0.29, and 0.17, respectively. The values of b_α for the same nanocomposites are 15, 6, 2.7, and 2.4 [5]. The dependences of k and cb_α on the nanofiller particle diameter D_{p} for these nanocomposites are presented in Fig. 6a. Because Eqns (13) and (14) give the value of ϑ in arbitrary units due to the use of the noninteger dimension d_s, k is assumed to equal $50/m_0^{3/d_{\text{s}}}$. The data of Fig. 6a suggest a close correspondence between $k(D_{\text{p}})$ and $cb_\alpha(D_{\text{p}})$ dependences calculated in the framework of the thermodynamic and fractal concepts, respectively. The values of k and cb_α very rapidly decrease as D_{p} grows, which suggests a lowering of interfacial adhesion. A dependence of this type indicates that the nanoadhesion effect under consideration is a true nanoeffect [38]. This inference is

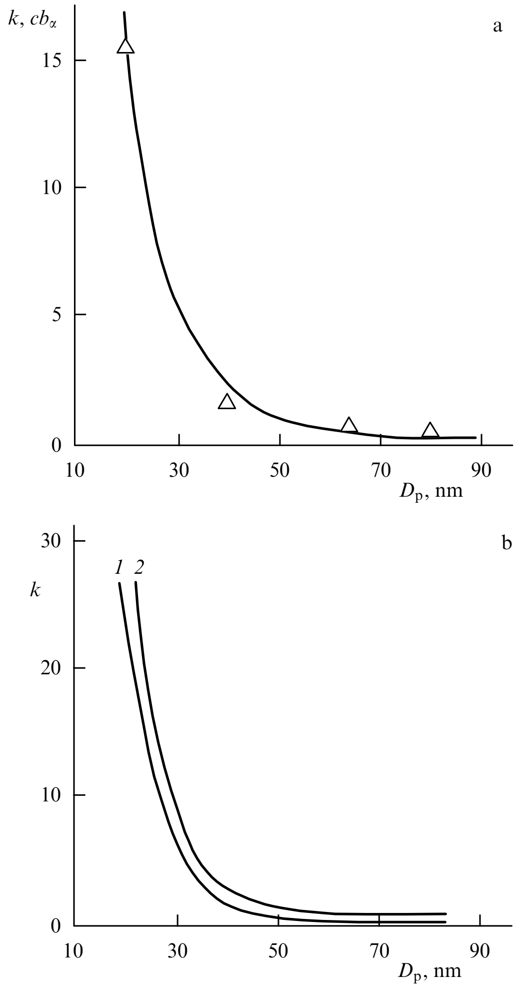

Figure 6. (a) Dependences of parameters k (solid line) and cb_α (triangles) on nanofiller particle diameter D_{p} [50]. (b) Dependences of parameter k on nanofiller particle diameter D_{p}, calculated at the limiting values of dimension $d_{\text{s}} = 2$ (*1*) and 3 (*2*) [51].

supported by calculations of $k(D_p)$ dependences, where k equals $50/m_0^{3/d_s}$, for two limiting values of $d_s = 2$ and 3. These dependences (Fig. 6b) are so close that they can be approximated for practical purposes by a single correlation (cf. Fig. 5b). Thus, the key factor determining the magnitude of the nanoadhesion effect is the particle diameter D_p, which supports the earlier conclusion about the dimensional origin of this effect [5].

The above findings confirmed once again that the nanoadhesion effect is of a purely dimensional nature, i.e., a true nanoeffect. Its description in the framework of the thermodynamic and fractal concepts revealed their excellent correspondence. An important factor influencing the interfacial adhesion level is the aggregation of nanofiller particles.

To conclude this section, let us estimate the temperature dependence of the interfacial adhesion level characterized by parameter b_α for particulate-filled phenylone/aerosyl nanocomposites. The authors of Ref. [54] obtained the following generalized correlation between the difference $\Delta\alpha_c$ in the values of thermal expansion coefficient α_c for nanocomposites and α_m for matrix polymer (phenylone), nanofiller content W_n (in mass %), and parameter b_α:

$$\frac{\Delta\alpha_c}{W_n} = 2.5 \times 10^{-4} b_\alpha\,, \tag{19}$$

which permits us to calculate the temperature variation of b_α. Figure 7 depicts dependences $b_\alpha(T)$ for two phenylone/aerosyl nanocomposites, allowing us to reach the following conclusions. First, the interfacial adhesion level in phenylone/aerosyl-MF nanocomposites with suppressed aerosyl particle aggregation is much higher than in phenylone/aerosyl nanocomposites where such aggregation occurs. Second, a rise in temperature leads to a reduction in b_α; the value of b_α for phenylone/aerosyl nanocomposites at high temperatures T falls to that in microcomposites. Third, a sharp rise in b_α at vitrification temperature T_g is observed only in the case of nanoadhesion, which means that the sharp increase in molecular mobility at T_g can elevate the interfacial adhesion level only in the case of complete contact between the polymer and the nanofiller [54].

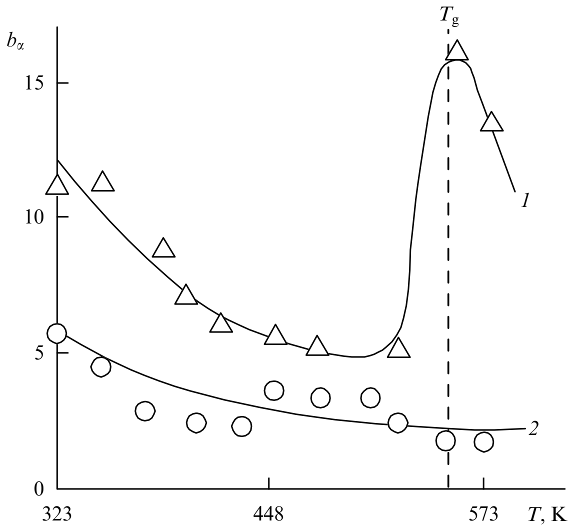

Figure 7. Dependences of parameter b_α on the test temperature T for phenylone/aerosyl-MF (*1*) and phenylone/aerosyl (*2*) nanocomposites. Vertical dashed line indicates vitrification temperature T_g [54].

2.3 Practical aspects of realization of nanoadhesion effect

Let us touch upon the practical aspects of the realization of the nanoadhesion effect in polymer nanocomposites. The 'effective clay particle' concept that has been proposed for polymer/organoclay nanocomposites concerns not only the layered nanofiller proper but also the adjacent layers of the polymer matrix (or those enclosed between intercalated silicate plates) [2]. A similar approach was applied by the authors of Refs [3, 55] to describing the reinforcement of polymer nanocomposites in general. The degree of reinforcement E_n/E_m of polymer nanocomposites is described in the framework of the percolation theory by the following equation [56]

$$\frac{E_n}{E_m} = 1 + 11\varphi_n^{1.7}\,, \tag{20}$$

where E_n and E_m are the elastic moduli of the composite and the initial matrix polymer, respectively.

A variant of relationship (20) modified with respect to nanocomposites has the form [5]

$$\frac{E_n}{E_m} = 1 + 11(\varphi_n + \varphi_{int})^{1.7}\,. \tag{21}$$

This equation implies that the concept dealt with in Ref. [55] considers a nanoparticle proper and the surrounding interface layer as the 'effective nanofiller particle', regardless of its nature. Then, the sum $(\varphi_n + \varphi_{int})$ should be regarded as the effective volumetric filling degree φ_n^{eff} [57].

The fractal model of interface layer formation in polymer nanocomposites leads to a simple relationship between parameters φ_{int} and φ_n [58]:

$$\varphi_{int} = c\varphi_n\,, \tag{22}$$

where coefficient c can vary in a rather broad range, depending on nanofiller particle geometry and surface structure, and also on polymer matrix molecular characteristics. A very important aspect of the problem is worthy of note. Both the effective clay particle concept [2] and the fractal model of interface layer formation [58] imply perfect adhesion between the polymer matrix and the nanofiller. In the context of the interpretation made in Section 1, perfect adhesion meets the condition $\alpha_c = \alpha_c^T$ or the criterion $b_\alpha = 1.0$ [to proceed from Eqn (3)]. In fact, the two interpretations disregard the influence of interfacial adhesion on the properties of polymer nanocomposites. It is their major disadvantage for the aforementioned reasons [18]. As shown in Ref. [37], the thickness of the interfacial layer is proportional to the adhesion strength, which makes it possible to take into account the interfacial adhesion level using the simple equation (18).Then, the effective volumetric filling degree φ_n^{eff} can be written out in the following form [59]

$$\varphi_n^{eff} = \varphi_n + \varphi_{int} = \varphi_n + cb_\alpha\varphi_n = \varphi_n(1 + cb_\alpha)\,. \tag{23}$$

The last equation clearly demonstrates the influence of the adhesion (nanoadhesion) level on the nanocomposite properties. A simple calculation shows that a rise in b_α from 1 to 15 at equal c, i.e., realization of the nanoadhesion effect, increases φ_n^{eff} by roughly one order of magnitude.

In the last 15 years, much attention has been given to polymer/organoclay nanocomposites [60], which have the key

Table 1. Variations in the properties of phenylone/aerosyl-MF nanocomposites containing 0.3 mass % of aerosyl and polymer/organoclay nanocomposites [59].

Property	Nanocomposite	
	phenylone/aerosyl-MF	polymer/organoclay
E_c, MPa	239	390 for PBT/MMT-3.0 [60]
$T_{5\%}$, K	35	17 for PBT/MMT-3.0 [60]
α_c, %	33	52 for PA-6/MMT-4.7 [40]
ε_f, %	56	62 for PP/MMT-2.5 [4]
A_p, %	6.1	15 for PA-6/MMT-4.7 [40]

Note: numerals with the conventional notations of polymer/organoclay nanocomposites denote Na^+-montmorillonite content expressed in mass %.

advantage of a roughly tenfold lower filler content than traditional composites, to which it imparts the same properties. The above estimate shows that nanocomposites exhibiting the nanoadhesion effect (at high enough $b_\alpha > 10$) match up with polymer/organoclay nanocomposites exactly as the latter do with traditional composites. To substantiate this inference, Table 1 presents the main characteristics of phenylone/aerosyl-MF nanocomposites containing 0.3 mass % of aerosyl, and polymer/organoclay nanocomposites with rather similar molecular characteristics of the polymer matrix and phenylone, which contain from 3.0 to 4.7 mass % of organoclay. It follows from a comparison of variations in elastic modulus $b_\alpha > 10$, temperature $T_{5\%}$ for the onset of thermal destruction, thermal expansion coefficient α_c, stress-at-break ε_f, and impact toughness A_p for phenylone/aerosyl-MF nanocomposites, on the one hand, and polybutylene-terephthalate/montmorillonite (PBT/MMT), polyamide-6/montmorillonite (PA-6/MMT), and polypropylene/montmorillonite (PP/MMT), on the other hand, that these characteristics are commensurate for such pairs of nanocomposites, although the aerosyl content in the former one is 10 times or more lower than the MMT content in polymer/organoclay nanocomposites.

It should be noted that the reduction in the thermal expansion coefficient has practical implications. First, this parameter is intrinsically high in polymers and can be an order of magnitude higher than in other materials [36]. Therefore, polymer articles operating in contact with such materials as metals or concrete may undergo deformation and decomposition under the effect of varying temperature. Second, the discrepancy between thermal expansion coefficients of the filler and the polymeric matrix in polymer composites causes deformation of interfacial layers and thereby negatively affects the properties of such composites. Evidently, the introduction of small amounts of a disperse nanofiller under conditions of realizing the nanoadhesion effect may eliminate or weaken this undesirable effect [59].

2.4 Interfacial regions as a reinforcement element of polymer nanocomposites

Equation (21) suggests that interfacial regions, along with the nanofiller proper, serve as a reinforcement element of the polymer nanocomposite structure. It is a purely theoretical conjecture based on the postulate of 'freezing' the molecular mobility of the nanofiller particles near the polymer matrix surface [61]. This postulate was verified experimentally in Ref. [62] by modern nanoscopic techniques by the example of butadiene–styrene rubber (BSR) samples filled with the nanoscale fullerene-containing mineral nanoshungite [63]. The nanostructure of the BSR/nanoshungite nanocomposite was studied using Nano-DST (Pacific Nanotechnology, USA) and Easy Scan DFM (Nanosurf, Switzerland) atomic-force microscopes by the semicontact method in the force modulation mode. The results of atomic-force microscopy were processed with the aid of a specialized SPIP software package (scanning probe image processor, Denmark) [62, 63].

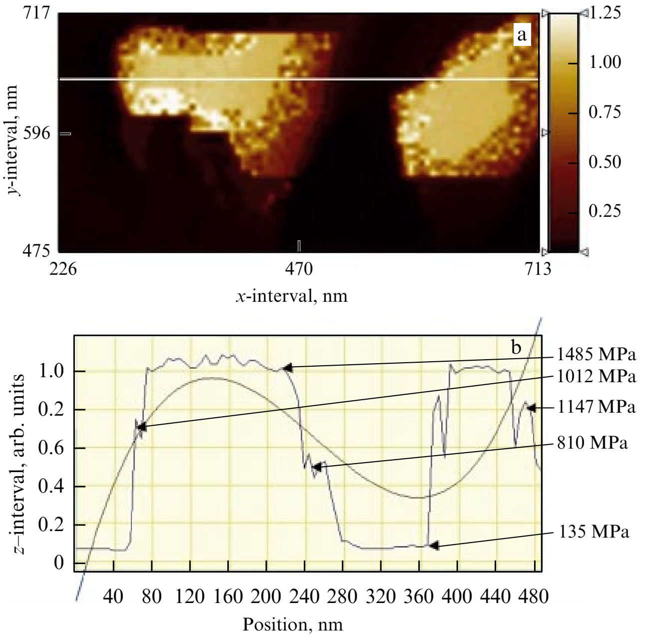

Figure 8. (a) A SPIP-treated image of butadiene–styrene rubber/nanoshungite nanocomposite, obtained by the force modulation method, and (b) mechanical characteristics of structural components according to the data of nanoindentation (150-nm strain) [62].

Figure 8 presents the results of calculations of elastic moduli for the components of the BSR/nanoshungite nanocomposite (matrix, nanofiller particles, and interfacial layers) based on interpolation of nanoindentation data. SPIP processing of an image of the polymer nanocomposite containing shungite nanoparticles allows the determination of the thickness l_{int} of the interfacial layer from the experimental data, which is represented in Fig. 8b as steps at the elastomer matrix–nanofiller interface. The measurement of the widths of 34 such steps (interface layers) in the SPIP-treated images of interfacial layer cross sections yielded the mean experimental value of $l_{\text{int}} = 8.7$ nm. Moreover, the results of nanoindentation (MPa values to the right in Fig. 8b) indicated that the elastic modulus of interfacial layers is only 23–45% lower than that of the nanofiller but 6.0–8.5 times higher than the modulus of elasticity of the polymer matrix. These experimental data confirm that the interfacial layer of the nanocomposite being studied serves as a reinforcement element, like the nanofiller proper [5, 61].

Then, the authors of Ref. [62] theoretically found the value of l_{int} by two methods and compared it with experimental data. One method simulated the interfacial layer in polymer composites as a result of the interaction of the polymer matrix with the nanofiller surface [20, 24]. In this case, there is a single linear scale l determining the interpenetration depth of these two fractals [64]. The filler elastic modulus being much higher (eleven-fold) than that of rubber (see Fig. 8b), their interaction reduces to the penetration of the filler surface into the polymer matrix, resulting in $l = l_{\text{int}}$. In this case, the following relationship holds [64]:

$$l_{\text{int}} \approx a\left(\frac{r_{\text{p}}}{a}\right)^{2(d-d_{\text{s}})/d}, \tag{24}$$

where a is the lower linear scale of the fractal behavior assumed to be equal for polymers to the statistical segment length l_{st} [65], and r_{p} is the nanofiller particle (or more precisely particle aggregate) radius (167.5 nm for nanoshungite) [63].

Length l_{st} is defined as follows [66]:

$$l_{\text{st}} = l_0 C_{\infty}, \tag{25}$$

where l_0 is the skeletal bond length in the main chain, equaling 0.154 nm for the two BSR blocks [67], and C_{∞} is the characteristic ratio standing for the statistical flexibility of the polymer chain [68]. For BSR, one has $C_{\infty} = 12.5$ [62].

The fractal dimension d_{s} of the nanoshungite surface can be found by using Eqn (7), and the specific surface S_{u} of this nanofiller from formula [56]

$$S_{\text{u}} = \frac{3}{\rho_{\text{n}} r_{\text{p}}}, \tag{26}$$

where ρ_{n} is the density of nanoshungite particle aggregates calculated from Eqn (15).

Calculations from Eqns (7), (15), and (26) give $d_{\text{s}} = 2.44$. The use of estimated parameters thus obtained and Eqn (24) yields the theoretical value of the interfacial layer thickness $l_{\text{int}}^{\text{theor}} = 7.8$ nm fairly close to the experimental one, the discrepancy in $l_{\text{int}} - l_{\text{int}}^{\text{theor}}$ being $\sim 10\%$.

The second approach to the estimation of $l_{\text{int}}^{\text{theor}}$ consists in using two equations [69]

$$\varphi_{\text{int}} = (d_{\text{s}} - 2)\,\varphi_{\text{n}}, \tag{27}$$

$$\varphi_{\text{int}} = \varphi_{\text{n}}\left[\left(\frac{r_{\text{p}} + l_{\text{int}}^{\text{theor}}}{r_{\text{p}}}\right)^3 - 1\right], \tag{28}$$

where φ_{int} and φ_{n} are the relative volume fractions of the interfacial regions and the nanofiller, respectively. Combining these equations allows the following formula for $l_{\text{int}}^{\text{theor}}$ to be obtained [62]:

$$l_{\text{int}}^{\text{theor}} = r_{\text{p}}\left[(d_{\text{s}} - 1)^{1/3} - 1\right]. \tag{29}$$

Calculating according to formula (29) gives the result $l_{\text{int}}^{\text{theor}} = 10.8$ nm for the nanocomposite of interest, in excellent agreement with the experiment as well (the discrepancy between l_{int} and $l_{\text{int}}^{\text{theor}}$ is $\sim 19\%$).

To conclude, an important experimental finding should be mentioned that follows from the SPIP-treated results of scanning the nanocomposite surface (Fig. 8b). It can be seen that a single surface of a nanoshungite particle may have from one to three (mean: two) steps structurally identifiable as interfacial layers. Characteristically, the width of these steps (or l_{int}) is roughly equal to the width of the first (nearest to the surface) step. This means that two (on the average) interfacial layers are formed in elastomer nanocomposites. One is due to the interaction between the nanofiller particle surface and the elastomer matrix resulting in freezing molecular mobility in this layer and its turning into a vitreous state. The other arises from the interaction between the vitreous interfacial layer and the elastomer polymer matrix. Of practical importance in this case is to elucidate if only one or both interfacial layers serve as the reinforcement element of the nanocomposite. The following calculations were needed to answer this question. The degree of reinforcement of polymer nanocomposites ($E_{\text{n}}/E_{\text{m}}$) is given by Eqn (21) in which the sum ($\varphi_{\text{n}} + \varphi_{\text{int}}$), in accordance with Eqn (27) equals [62]

$$\varphi_{\text{n}} + \varphi_{\text{int}} = \varphi_{\text{n}}(d_{\text{s}} - 1), \tag{30}$$

if only one interfacial layer (nearest to the nanoshungite surface) is the reinforcement element, and

$$\varphi_{\text{n}} + 2\varphi_{\text{int}} = \varphi_{\text{n}}(2d_{\text{s}} - 3), \tag{31}$$

if both interfacial layers serve as the reinforcement element.

Calculations using Eqns (30) and (31) gave $E_{\text{n}}/E_{\text{m}}$ values of 4.60 and 6.65, respectively. The experimental value of $E_{\text{n}}/E_{\text{m}} = 6.10$ being close to that found from Eqn (31), this means that the reinforcement element in the nanocomposites of interest is formed by the two interfacial layers. For this reason, numerical coefficient 2 should be introduced into equations, e.g., Eqn (24), for determining l_{int} in nanocomposites with an elastomer matrix. To recall, Eqn (24) was initially derived as a relationship with the sign of proportionality, i.e., without fixing the proportionality coefficient [64], and the authors of Ref. [70] obtained coefficient 1.2 for the disperse filler.

Thus, the nanoscopic techniques employed by the authors of Ref. [62] made it possible to estimate not only the structural features of the interfacial layer in polymer nanocomposites but also this layer's size and properties. It was shown for the first time that particulate-filled elastomer nanocomposites form two or more consecutive layers that serve as the reinforcement element for these materials. Theoretical methods for the estimation of the interfacial layer thickness, developed in the framework of fractal analysis yield results in excellent agreement with available experimental data.

2.5 Nanofiller structure in a polymer matrix

It is well known [71, 72] that nanofiller particles make up linear spatial structures (chains) in particulate-filled elastomer nanocomposites (rubbers). At the same time, filler particles (or their aggregates) in polymer composites filled with disperse microparticles (microcomposites) form the backbone with fractal properties determining the structure of the polymer matrix (the analog of the fractal lattice in computer simulations) [24]. This difference accounts for different mechanisms underlying the formation of the polymer matrix structure in micro- and nanocomposites. The presence of the fractal particle (particle aggregates) backbone in the former leads to 'perturbation' of the polymer matrix structure, apparent as the enlargement of its fractal dimension d_{f} [24, 25]. In the latter case, variations of the nanofiller content do not affect the d_{f} value, which remains equal to the fractal dimension of the polymer matrix structure [5]. As expected, the difference between the structure formation mechanisms in these two classes of composite materials determines changes to their properties, e.g., degree of reinforcement.

A few methods (both experimental [73, 74] and theoretical [24]) are currently available for the study of the filler structure (distribution) in a polymer matrix. The data obtained by all these methods indicate that this distribution is characterized by the fractal dimension D_B of the nanofiller particle backbone. However, the correct definition of the fractal (Hausdorff) dimension of any object includes three compulsory conditions. The first is the aforementioned definition of the numerical value of the fractal dimension which should differ from the topological dimension of the object. Any real (physical) fractal is known to possess fractal properties only in a certain scale range [75]. Therefore, the second condition concerns the proof of the object's self-similarity within this range [76]. Finally, the third condition covers the correct choice of the measurement scale range itself. It is shown in Refs [77, 78] that the minimum range must contain at least one self-similarity iteration.

The authors of Ref. [79] estimated the dimension D_B both experimentally and theoretically and tackled the problem of fulfillment of the two aforementioned conditions [77, 78], i.e., they obtained strong evidence of the fractal backbone of filler particles (or their aggregates) in particulate-filled polymer nanocomposites exemplified by polypropylene/calcium carbonate (PP/$CaCO_3$).

Figure 9a demonstrates an electron micrograph of the cleavage plane in a PP/$CaCO_3$ nanocomposite with a mass content $W_n = 4$ mass % of $CaCO_3$. It clearly shows the presence of the filler particle (aggregate) distribution in the size range from ~ 80 nm (individual $CaCO_3$ particles) to 360 nm (aggregates), which dictates the necessity of the quantitative characterization of this distribution that was undertaken in Ref. [73] with the aid of dimension D_B.

The first method for the experimental determination of dimension D_B makes use of the following fractal relationship [80, 81]:

$$D_B = \frac{\ln N}{\ln \rho}\,, \tag{32}$$

where N is the number of particles with size ρ.

The particle sizes were determined by electron microscopy (see Fig. 9a). At least 200 particles of a PP/$CaCO_3$ nanocomposite were measured. They were allocated to 8 groups for which mean N and ρ values were derived. Then, the linearity of $N(\rho)$ dependence in double log-log coordinates was established and this allowed the value of D_B to be calculated from its slope (Fig. 9b). Obviously, the fractal dimension D_B is determined in this method in the two-dimensional Euclidean space, whereas the real nanocomposite needs to be considered in a three-dimensional Euclidean space. The following equation can be applied to recalculate D_B for a three-dimensional space:

$$D3 = \frac{d + D2 - \left[(d - D2)^2 - 2\right]^{1/2}}{2}\,, \tag{33}$$

where $D3$ and $D2$ are the fractal dimensions in three- and two-dimensional Euclidean spaces, respectively, and $d = 3$.

Dimension D_B calculated by this method amounts to 1.44, i.e., it characterizes more or less branched structures (chains) of nanofiller particles or their aggregates within a polymer nanocomposite. To recall, the value of D_B for particulate-filled polyhydroxyether/graphite microcomposites varies from ~ 2.30 to 2.80 [24]; in other words, the filler particle backbone in these materials exhibits a spatial rather than linear structure [75].

Another approach to experimental determination of D_B is the so-called 'box-counting technique' [83]. In this method, a grid composed of square boxes with a side length α_i ranging within 4.5–24 mm and a constant ratio $\alpha_{i+1}/\alpha_i = 1.5$ is imposed on the magnified micrograph of a nanocomposite (see Fig. 9a); then, the number of boxes N_i into which nanocomposite particles fall is counted, either wholly or in part. Five arbitrary grid positions with respect to the micrograph were chosen for each measurement. The following equation must be satisfied if the nanofiller particle backbone has a fractal dimension [83]:

$$N_i \sim S_i^{-D_B/2}\,, \tag{34}$$

where S_i is the box area equal to α_i^2.

Figure 9c shows the S_i dependence of N_i in double logarithmic coordinates for a PP/$CaCO_3$ nanocomposite, corresponding to relation (34). As may be seen from this figure, the linearity of the dependence allows D_B to be determined from its slope. Its value of 1.23 suggests good correspondence of D_B dimensions measured by the two methods, with the discrepancy being $\sim 15\%$ after their recalculations for a three-dimensional space according to Eqn (33).

It was shown in paper [84] that the following condition should be fulfilled for self-similar fractal objects when relationship (34) is used:

$$N_i - N_{i-1} \sim S_i^{-D_B}\,. \tag{35}$$

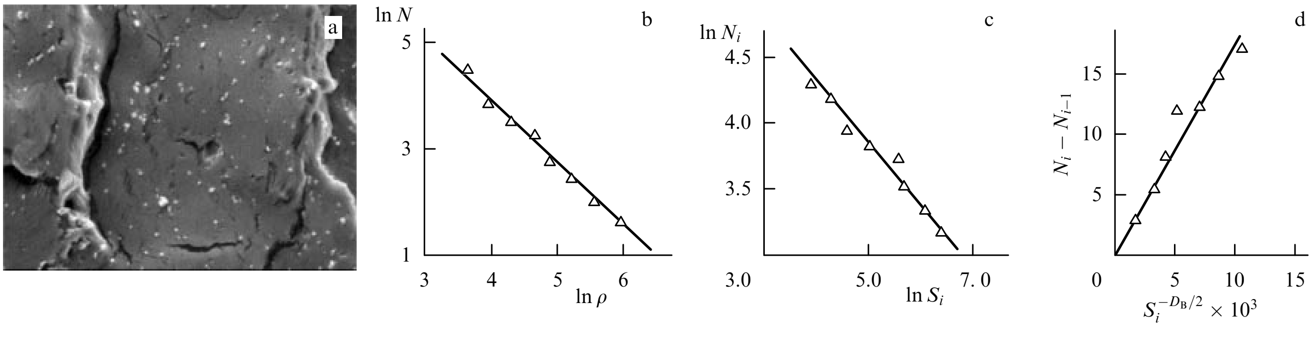

Figure 9. (a) Electron micrograph of a cleavage face of PP/$CaCO_3$ nanocomposite with the nanofiller content $W_n = 4$ mass %. (b) Dependence of the number N of nanoparticles on their size ρ in a PP/$CaCO_3$ nanocomposite with $W_n = 4$ mass %. (c) Dependence of the number of covering squares N_i on their area S_i corresponding to relation (34) for a PP/$CaCO_3$ nanocomposite with $W_n = 4$ mass %. (d) Dependence of $N_i - N_{i-1}$ on $S_i^{-D_B/2}$ corresponding to relation (35) for a PP/$CaCO_3$ nanocomposite with $W_n = 4$ mass % (taken from Ref. [79]).

Figure 9d illustrates the dependence corresponding to relation (35) for the PP/CaCO$_3$ nanocomposite being considered. Evidently, this linear dependence passes through the origin of coordinates, which confirms, in accordance with Eqn (35), the statistical self-similarity of the particle chains or aggregates in the chosen range of α_i [84].

Given the magnified micrograph in Fig. 9a, the data of Fig. 9d suggest a self-similarity interval of $\sim 427-2180$ nm for CaCO$_3$ chains. In due course, the distance λ between nanofiller particles can be calculated as follows [5]:

$$\lambda = \left[\left(\frac{4\pi}{3\varphi_{\mathrm{n}}}\right)^{1/3} - 2\right]\frac{D_{\mathrm{p}}}{2}\,, \tag{36}$$

where φ_{n} is the volume content of the nanofiller, and D_{p} is the diameter of its particles.

The calculation using Eqns (15) and (36), where quantity φ_{n} is defined as [5]

$$\varphi_{\mathrm{n}} = \frac{W_{\mathrm{n}}}{\rho_0}\,, \tag{37}$$

gives $\lambda = 95$ nm, i.e., the self-similarity interval of the nanofiller particle backbone includes, as expected, a few particles (or their aggregates).

It was shown in Refs [77, 78] that the minimum measurement scale range S_i must contain at least one self-similarity iteration. This being the case, the condition for the ratio of maximum ($S_{\max}$) to minimum ($S_{\min}$) covering square areas must be fulfilled [78]:

$$\frac{S_{\max}}{S_{\min}} > 2^{2/D_{\mathrm{B}}}\,. \tag{38}$$

Therefore, in the case being considered, $S_{\max}/S_{\min} = 576/20.25 = 28.4$ or is higher than $2^{2/D_{\mathrm{B}}} = 2.07$ for the PP/CaCO$_3$ nanocomposite. This means that the measurement scale range was correctly chosen [77].

The number μ of self-similarity iterations can be estimated from the inequality [78]

$$\left(\frac{S_{\max}}{S_{\min}}\right)^{D_{\mathrm{B}}/2} > 2^{\mu}\,. \tag{39}$$

Using the above values of parameters in inequality (39) gives $\mu = 2.30$ for the PP/CaCO$_3$ nanocomposite, meaning that the number of self-similarity iterations under the experimental conditions of Ref. [79] is higher than unity, which confirms once again the correctness of D_{B} evaluation [74].

Let us consider the physical causes responsible for lower D_{B} values in polymer nanocomposites than in analogous microcomposites, i.e., the causes behind the formation of the first branched chains (aggregates) of the nanofiller particles. The value of D_{B} can be found theoretically in accordance with the equation [24]

$$\varphi_{\mathrm{int}} = \frac{D_{\mathrm{B}} + 2.55d_0 - 7.10}{4.18}\,, \tag{40}$$

where φ_{int} is the relative fraction of interfacial regions, and d_0 is the dimension of the initial nanofiller particle surface.

The d_0 values were estimated using Eqns (26), (7), and those of φ_{int} from formula (27). The theoretical value of D_{B} found from Eqn (40) is ~ 1.10, in fairly good agreement with the above experimental estimates of this parameter. Equation (40) unambiguously indicates the causes of lower D_{B} in nanocomposites than in microcomposites: high $d_0 = 2.60$ (compared with 2.17 [42] for graphite microparticles), and low φ_{n}, which accounts for small φ_{int} values [see Eqn (22)].

Thus, the above findings indicate that branched chains of nanofiller particles (particle aggregates) in polymer nanocomposites are physical fractals within a self-similarity (and, consequently, fractality [81]) range from ~ 4.27 to 2180 nm. The dimension D_{B} of their structure in this range can be estimated both in experiment and theoretically in accordance with relations (32), (34), and (40). The small dimensions of the filler particle (aggregate) backbone structure in polymer nanocomposites are due to the high fractal dimension of the initial nanofiller particle surface and the low nanofiller content.

2.6 Aggregation of nanofiller particles

At present, one of the most reliable and cost-effective methods for the improvement of the mechanical properties of polyethylenes is their doping with various organic or inorganic fillers. One of them is calcium carbonate, which has long been used for this purpose, largely in the production of various polyolefin films applied in a variety of ways to optimize equipment performance, impart the properties of whiteness or dullness to all kinds of surfaces, and facilitate overprinting. However, calcium carbonate with micrometer-size particles is an inert filler and only weakly influences the mechanical properties of the nanocomposites thus obtained. The introduction of CaCO$_3$ nanoparticles, even together with a binding agent, does not necessarily improve the situation [85–87]. It was shown in Ref. [88] that the relatively low degree of reinforcement of polymer nanocomposites filled with CaCO$_3$ nanoparticles is due to the low interfacial adhesion level and nanoparticle aggregation. The authors of Ref. [89] studied nanofiller aggregation and its influence on the level of interfacial adhesion in low-density polyethylene/calcium carbonate (LDPE/CaCO$_3$) nanocomposites.

The authors of Ref. [90] considered the three main cases of the dependence of reinforcement degree $E_{\mathrm{c}}/E_{\mathrm{m}}$ (where E_{c} and E_{m} are the moduli of elasticity of the composite and the matrix polymer, respectively) on the nanofiller volume content φ_{n}. They distinguished the following main types of $E_{\mathrm{c}}/E_{\mathrm{m}}(\varphi_{\mathrm{n}})$ dependences:

(1) perfect adhesion between the nanofiller and the polymer matrix described by the Kerner equation, which can be approximated by the following equation

$$\frac{E_{\mathrm{c}}}{E_{\mathrm{m}}} = 1 + 11.6\varphi_{\mathrm{n}} - 44.4\varphi_{\mathrm{n}}^2 + 96.3\varphi_{\mathrm{n}}^3\,; \tag{41}$$

(2) zero adhesion strength with a large friction coefficient between nanofiller and polymer matrix, satisfying the equation

$$\frac{E_{\mathrm{c}}}{E_{\mathrm{m}}} = 1 + \varphi_{\mathrm{n}}\,, \quad \text{and} \tag{42}$$

(3) complete absence of interaction and an ideal slip between nanofiller and polymer matrix when the modulus of elasticity of the composite actually depends on the polymer cross section and is related to the degree of filling by the equation

$$\frac{E_{\mathrm{c}}}{E_{\mathrm{m}}} = 1 - \varphi_{\mathrm{n}}^{2/3}\,. \tag{43}$$

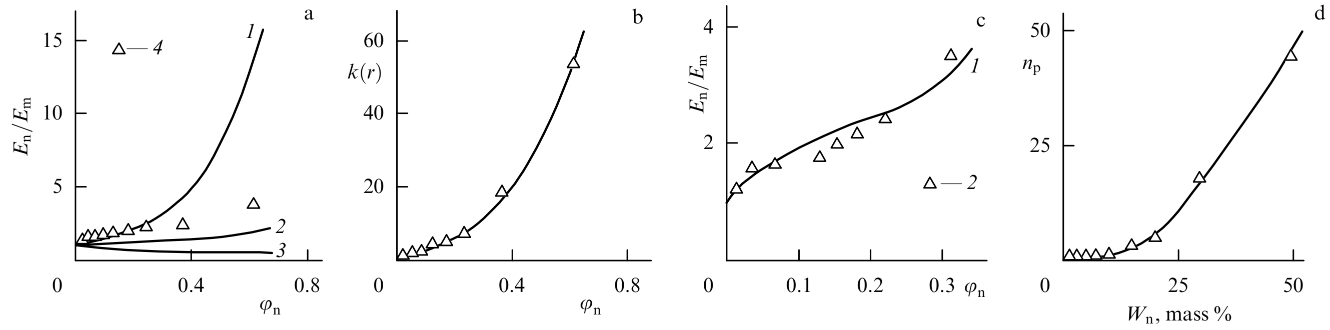

Figure 10. (a) Dependences of reinforcement degree E_n/E_m on nominal nanofiller volume content φ_n: *1–3* — theoretical dependences corresponding to Eqns (41)–(43), and *4* — experimental data for LDPE/CaCO$_3$ nanocomposites. (b) Dependence of aggregation parameter $k(r)$ on nanofiller volume content φ_n for LDPE/CaCO$_3$ nanocomposites. (c) Dependence of reinforcement degree E_n/E_m on real nanofiller volume content φ_n: *1* — calculation from Eqn (41), and *2* — experimental data for LDPE/CaCO$_3$ nanocomposites. (d) Dependence of the number n_p of initial CaCO$_3$ particles in one aggregate on nanofiller mass content W_n for LDPE/CaCO$_3$ nanocomposites (taken from Ref. [89]).

Figure 10a compares E_c/E_m dependences computed from Eqns (41)–(43) and obtained in experiment for LDPE/CaCO$_3$ nanocomposites. As may be seen, at a low CaCO$_3$ content (up to $W_n = 15$ mass % or $\varphi_n = 0.185$, inclusive), the experimental data agree with Eqn (41); the discrepancy becomes apparent at higher W_n (or φ_n) and increases with increasing W_n.

The discrepancy between theory and experiment may be due to two causes: either aggregation of the initial CaCO$_3$ particle or a decreased interfacial adhesion level. Let us consider both of them. The degree of aggregation of initial nanofiller particles can be estimated in the framework of the dispersion strength theory [91], where the yield stress τ_n per nanocomposite shear is defined as

$$\tau_n = \tau_m + \frac{G b_B}{\lambda} \,. \tag{44}$$

Here, τ_m is the yield stress per polymer matrix shear, G is the shear modulus, b_B is the Burgers vector, and λ is the distance between nanofiller particles.

In the case of nanofiller particle aggregation, Eqn (44) assumes the form [91]

$$\tau_n = \tau_m + \frac{G b_B}{k(r)\,\lambda} \,, \tag{45}$$

where $k(r)$ is the aggregation parameter.

The parameters entering in formulas (44) and (45) are defined as described below. The general ratio of normal stress σ to shear stress τ has the form [92]

$$\tau = \frac{\sigma}{\sqrt{3}} \,. \tag{46}$$

Young's modulus E and shear modulus G are related as [69]

$$G = \frac{E}{d_f} \,, \tag{47}$$

where d_f is the fractal dimension of the nanocomposite structure, defined by the equation [75]

$$d_f = (d-1)(1+\nu) \,. \tag{48}$$

Here, d is the dimension of the Euclidean space in which the fractal is considered (in our case, obviously, $d = 3$), and ν is the Poisson's ratio estimated from the results of mechanical tests using the relationship [93]

$$\frac{\sigma_y}{E_n} = \frac{1-2\nu}{6(1+\nu)} \,, \tag{49}$$

where $\sigma_y$is the nanocomposite yield stress.

The Burgers vector b_B for polymer materials is defined as follows [94]:

$$b_B = \left(\frac{60.5}{C_\infty}\right)^{1/2} \ [\text{Å}] \,, \tag{50}$$

where C_∞ is the characteristic ratio related to dimension d_f through the equation [94]

$$C_\infty = \frac{2 d_f}{d(d-1)(d-d_f)} + \frac{4}{3} \,. \tag{51}$$

Figure 10b shows the dependence of aggregation parameter $k(r)$ on φ_n for LDPE/CaCO$_3$ nanocomposites. It can be seen that $k(r)$ begins to rapidly grow for $\varphi_n > 0.185$, which suggests a sharp rise in aggregation of initial nanofiller particles provided their content is sufficiently high. The distance λ between nanofiller particles can be found from Eqn (36), while the combination of Eqns (15), (36), and (37) allows the following relationship to be obtained:

$$k(r)\,\lambda = \left[\left(\frac{0251\pi D_{ag}^{1/3}}{W_n}\right)^{1/3} - 2\right] \frac{D_{ag}}{2} \,, \tag{52}$$

which makes it possible to determine the true diameter D_{ag} of CaCO$_3$ aggregates taking into account the aggregation of nanofiller particles. Then, Eqns (15) and (37) can be used to calculate the real values of ρ_0 (ρ_n) and φ_n, respectively. Next, the use of real φ_n values permits us to obtain theoretical dependence $E_n/E_m(\varphi_n)$ in accordance with Eqn (41). Such a dependence and the respective experimental data for LDPE/CaCO$_3$ nanocomposites are presented in Fig. 10c. Thus, this computational method yields excellent agreement between theory and experiment over the entire range of W_n, which suggests perfect (in terms of Kerner's model) adhesion between LDPE and CaCO$_3$, regardless of the degree of nanoparticle aggregation.

The degree of nanofiller particle aggregation is also possible to evaluate from the mean number n_p of initial

$CaCO_3$ particles per aggregate using the equation [56]

$$R_{\mathrm{ag}} = \left(\frac{n_{\mathrm{p}} S_{\mathrm{p}}}{\pi \eta} \right)^{1/2} , \tag{53}$$

where R_{ag} is the radius of an aggregate of nanofiller particles determined from Eqn (52), S_{p} is the cross section area of an initial nanoparticle, and η is the packing density equal to 0.74 for monodisperse rings [56].

Figure 10d depicts the dependence of n_{p} on $CaCO_3$ mass content W_{n} for LDPE/$CaCO_3$ nanocomposites. As expected, a sharp increase in n_{p} originates at $W_{\mathrm{n}} = 15$ mass %, while at $W_{\mathrm{n}} = 50$ mass % the mean number of nanoparticles per aggregate already exceeds 40.

Let us analyze here the alteration of the interfacial adhesion level for the nanocomposites of interest. The authors of Ref. [89] evaluated this variable using parameter b_{f} found from the equation [95]

$$\sigma_{\mathrm{f}}^{\mathrm{n}} = \sigma_{\mathrm{f}}^{\mathrm{m}} K_{\mathrm{v}} - b_{\mathrm{f}} \varphi_{\mathrm{n}} , \tag{54}$$

where $\sigma_{\mathrm{f}}^{\mathrm{n}}$ and $\sigma_{\mathrm{f}}^{\mathrm{m}}$ are the fracture stresses of the nanocomposite and polymer matrix, respectively, and K_{v} is the stress concentration coefficient. Obviously, because an increase in b_{f}, unlike that of parameter b_{α} in Eqn (3), leads to $\sigma_{\mathrm{f}}^{\mathrm{n}}$ decreasing, it implies that the interfacial adhesion level decreases, too [96].

The quantity $\sigma_{\mathrm{f}}^{\mathrm{m}}$ is assumed to be equal to the strength of the matrix polymer (for LDPE, $\sigma_{\mathrm{f}}^{\mathrm{m}} = 12$ MPa), and quantity K_{v} is determined from the equation [96]

$$\sigma_{\mathrm{f}}^{\mathrm{n}} = \sigma_{\mathrm{f}}^{\mathrm{m}} (1 - \varphi_{\mathrm{n}}^{2/3}) K_{\mathrm{v}} . \tag{55}$$

Figure 11a exhibits the dependence $b_{\mathrm{f}}(W_{\mathrm{n}})$ for LDPE/$CaCO_3$ nanocomposites, which suggests even a slight decrease in b_{f} (increased interfacial adhesion level) at $W_{\mathrm{n}} = 1-3$ mass %, after which b_{f} remains roughly constant and equal to ~ 39. To recall, this is a high enough level of interfacial adhesion. Thus, the value of b_{f} varies from 36 to 132 for polypropylene/organoclay nanocomposites with binding agents [3]. A similar calculation for LDPE/$CaCO_3$ nanocomposites with stearic acid as the binding agent [85] gave $b_{\mathrm{f}} = 136$. This confirms the conjecture made by the authors of Ref. [88] that a relatively low interfacial adhesion level may be the cause of the low reinforcement degree in $CaCO_3$-filled nanocomposites. Moreover, a comparison of the data in Figs 10a, b, d and Fig. 11a points to the fact that the sole cause of lowering the experimental reinforcement degree relative to the theoretically possible value is the aggregation of nanofiller particles, which is from a practical standpoint equivalent to a fall in φ_{n} (twofold for $W_{\mathrm{n}} = 50$ mass %) [89].

Let us next consider the practical aspect of using disperse particles as nanofillers. Figure 11b illustrates dependences of the reinforcement degree $E_{\mathrm{n}}/E_{\mathrm{m}}$ on the nanofiller mass content W_{n} for polypropylene/Na^+-montmorillonite (PP/MMT) [4] and LDPE/$CaCO_3$ nanocomposites. It follows from a comparison of these dependences that at low W_{n} (< 25 mass %) the PP/MMT nanocomposites have higher $E_{\mathrm{n}}/E_{\mathrm{m}}$ ratios at equal W_{n}, but the situation reverses as W_{n} increases further. Moreover, it should be borne in mind that particulate-filled nanocomposites are easier to process and cheaper to produce. Exfoliation of organoclay in an amount over 10 mass % encounters difficulty; therefore, the dependence $E_{\mathrm{n}}/E_{\mathrm{m}}(\varphi_{\mathrm{n}})$ for polymer/organoclay nanocomposites rapidly comes to asymptotic branch, as shown in Fig. 11b. Notice that suppression of disperse nanofiller particle aggregation may produce an even greater effect (Fig. 11b, curve *3*) and that there are some methods currently available in order to do so [5, 26, 97]. The relationship of dependences $E_{\mathrm{n}}/E_{\mathrm{m}}(\varphi_{\mathrm{n}})$ for particulate-filled polymer nanocomposites and polymer/organoclay nanocomposites illustrated in Fig. 11b was predicted theoretically in paper [98].

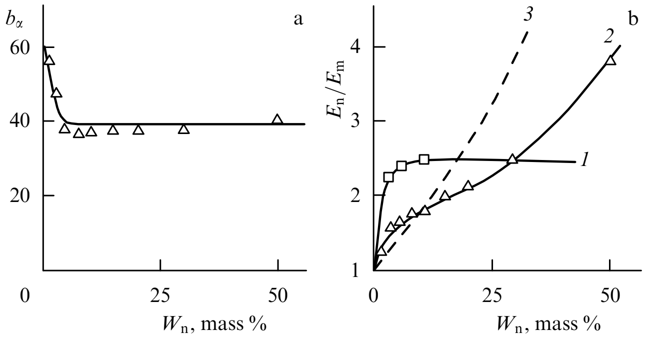

Figure 11. (a) Dependence of parameter b_{α} on nanofiller mass content W_{n} for LDPE/$CaCO_3$ nanocomposites. (b) Dependences of reinforcement degree $E_{\mathrm{n}}/E_{\mathrm{m}}$ on nanofiller mass content W_{n} for PP/MMT (*1*) and LDPE/$CaCO_3$ (*2*) nanocomposites; *3* — calculation in accordance with Eqn (41) (taken from Ref. [89]).

Thus, the above results give evidence that a decrease in the reinforcement degree in LDPE/$CaCO_3$ nanocomposites compared with the attainable theoretical value is due to initial nanofiller particle aggregation alone. In this case, the interfacial adhesion level remains rather high and roughly constant. From the practical standpoint, particulate-filled polymer nanocomposites are might be competitive with polymer/organoclay nanocomposites, especially if produced by simple enough and effective methods for the suppression of initial nanofiller particle aggregation.

3. Mechanical properties

3.1 Reinforcement degree

A variety of methods are currently in use to describe the reinforcement degree in polymer nanocomposites, i.e., the increase in the elastic modulus of a microcomposite compared with a matrix polymer. They include micromechanical [57, 96], percolation [56], and fractal [5, 24] models that are essentially different in that the first one involves the calculation of reinforcement degree by taking account of the nanofiller modulus of elasticity, whereas the last two disregard this parameter. The authors of Ref. [99] employed one of the many micromechanical models to describe the dependence of reinforcement degree on nanofiller content for propylene/carbon nanotube (PP/CNT) nanocomposites.

The reinforcement degree $E_{\mathrm{n}}/E_{\mathrm{m}}$ was described based on the Counto model (100):

$$\frac{E_{\mathrm{n}}}{E_{\mathrm{m}}} = (1 - \varphi_{\mathrm{n}}^{1/2}) + \frac{E_{\mathrm{m}}}{\left[(1 - \varphi_{\mathrm{n}}^{1/2}) / \varphi_{\mathrm{n}}^{1/2} \right] E_{\mathrm{m}} + E_{\mathrm{f}}} , \tag{56}$$

where E_{f} is the nanofiller modulus of elasticity.

Equation (56) implies perfect (in terms of the Kerner model) adhesion between the nanofiller and polymer matrix; it demonstrates that an increase in nanofiller modulus of elasticity E_{f} decreases its role in determining $E_{\mathrm{n}}/E_{\mathrm{m}}$ of a

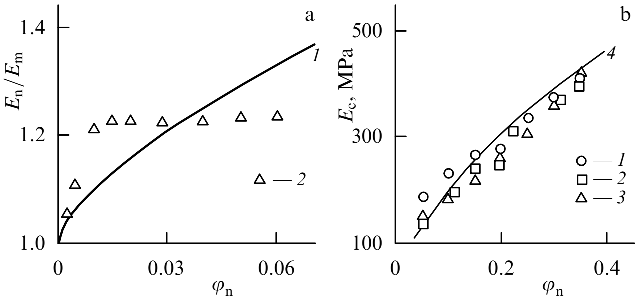

Figure 12. (a) Dependences of reinforcement degree E_n/E_m on nanofiller volumetric filling degree φ_n for PP/CNT nanocomposites: *1* — calculation in accordance with Eqn (56), and *2* — experimental data [99]. (b) Dependences of elastic modulus E_c on nanofiller content φ_n for LDPE/UHMWPE nanocomposites: *1–3* — calculation in accordance with Eqns (58), (60), and (20), respectively, and *4* — experimental data [102].

nanocomposite. This observation is particularly true of CNTs characterized by a very high modulus of elasticity amounting to 1000 GPa [9], but also holds for other (in particular, disperse) inorganic nanofillers. Thus, estimates based on Eqn (56) showed that the use of only the first term on the right-hand side of this equation at $E_n = 1.40$ GPa, $E_m = 0.95$ GPA, and $\varphi_n = 0.060$ gives as small an error as 0.1%. In other words, parameter E_f has practically no influence on the reinforcement degree in PP/CNT nanocomposites. The error increases as E_f decreases. However, it does not exceed $\sim 10\%$ even at $E_f = 10$ GPa (typical of disperse nanofillers) and other aforementioned values of the parameters.

Figure 12a compares experimental (dots) and theoretical [calculated from expression (56)] dependences $E_n/E_m(\varphi_n)$. Evidently, experimental E_n/E_m values at a low CNT content ($\varphi_n \leqslant 0.020$) exceed theoretical ones; this relationship becomes inverted for $\varphi_n \geqslant 0.040$. Let us consider the causes behind such a discrepancy. In the framework of the percolation theory, the value of E_n/E_m is given by Eqn (5):

$$\frac{E_n}{E_m} = 1 + 11(2.86\varphi_n b_\alpha)^{1.7}, \qquad (57)$$

where b_α is the parameter characterizing the interfacial adhesion level [see Eqn (3)].

Calculations according to Eqn (57) revealed a decrease in b_α from 5.09 to 0.21 within the range of $\varphi_n = 0.003 - 0.060$ for PP/CNT nanocomposites. Therefore, realization of the nanoadhesion effect for $\varphi_n \leqslant 0.020$ results in high E_n/E_m values [see Eqn (57)]. At $\varphi_n \approx 0.030$, regarded in the literature as the optimal CNT content [9], perfect adhesion is achieved, when theory and experiment give the same E_n/E_m values. For $\varphi_n \geqslant 0.040$, the interfacial adhesion level b_α falls to below 1.0, and theoretical E_n/E_m values calculated on the assumption of perfect adhesion exceed experimental ones.

This suggests a small role of the nanofiller elastic modulus even when micromechanical models are applied, and the assumption of perfect adhesion adopted in such models may result in a serious error in the calculation of the reinforcement degree [99].

Polymer/polymer composites (nanocomposites) represent a specific variety of this class of polymer materials with poorly known properties [3, 5, 6]. The authors of Ref. [101] considered the reinforcement mechanism operating in the polymer/polymer type composite low-density polyethylene/ultrahigh molecular weight polyethylene (LDPE/UHMWPE).

The simplest way of evaluating moduli of elasticity of composites reduces to using parallel and sequential models that specify the upper and lower bounds of the elastic modulus E_c, respectively. The parallel model implies homogeneous deformation in two composite phases, and the value of E_c is found from the following equation [96]

$$E_c = E_f\varphi_n + E_m(1 - \varphi_n), \qquad (58)$$

where E_f is the filler (UHMWPE in the case at hand) elastic modulus, and φ_n is the filler volume content.

Because polyethylene density is close to 1000 kg m^{-3} [102], the volume and weight contents of the filler can be regarded as equal to each other. Figure 12b compares experimental and theoretical [according to formula (58)] dependences $E_c(\varphi_n)$ for LDPE/UHMWPE composites. Evidently, they are in excellent agreement, which suggests that the upper limiting E_c values for these composites are reached, and therefore the homogeneous deformation in LDPE and UHMWPE is attained. To recall, for polymer composites filled with high-modulus ($E_f \gg E_m$) inorganic filler, the upper bound of E_c described by Eqn (58) is practically never reached, and the real E_c value is several-fold lower than that predicted by formula (58). Specifically, the experimental E_n value for PP/CNT nanocomposites is approximately 44 times lower than the one predicted by formula (58). The lower bound of E_c is defined in accordance with the sequential model as [96]

$$E_c = \frac{E_f E_m}{E_f(1 - \varphi_n) + E_m\varphi_n}. \qquad (59)$$

For PP/CNT nanocomposites, $E_c = 1.23$ GPa, in accordance with Eqn (59), and $E_c = 1.40$ in experiment (only a 12.5% difference). This means that the high elastic modulus of a filler (nanofiller) is not beneficial for the realization of a high reinforcement degree in composites (nanocomposites) for the obvious reason that the above difference between E_f and E_m precludes attainment of homogeneous deformation in both phases of a composite (nanocomposite). However, it is possible for the composites of interest, especially if deformation in the devitrified amorphous phase of LDPE and UHMWPE polymers is taken into account.

Another variant is a purely composite one, and E_c is calculated based on the principles of fractal analysis. Such calculation is possible to make using the equation [24]

$$E_c = (8.1D_f - 10.8)\,\sigma_y, \qquad (60)$$

where D_f is the dimension of the regions where the excess energy is localized, and σ_y is the yield stress.

This model implies [24] that a change in E_c is due to a change in the polymer matrix structure, and dimensions D_f and d_f are related through the equation [75]

$$D_f = 1 + \frac{1}{3 - d_f}, \qquad (61)$$

where the quantity d_f can be found from equation (48).

Figure 12b compares experimental and theoretical [according to formula (60)] dependences $E_c(\varphi_n)$ and demonstrates their excellent agreement, suggesting that the growth of E_c with increasing φ_n is due to structural changes in LDPE/UHMWPE composites.

An important aspect needs to be mentioned in conclusion. In accordance with Eqns (20) and (21), the E_n/E_m ratio can not be higher than 12, regardless of the filler modulus of elasticity. Such a result was obtained by the authors of Ref. [103] in experiments with hybrid composites filled with organoclay and short fibers.

An essential difference between micromechanical and percolation or fractal models describing the reinforcement degree in polymer nanocomposites lies in the fact that the first one takes into account the filler (nanofiller) modulus of elasticity, whereas the last two do not. Both the percolation [56] and fractal [5] reinforcement models suggest that the role of the filler (nanofiller) reduces to modification and fixation of the matrix polymer structure. Such a point of view is quite natural, bearing in mind the difference between elastic moduli of the filler (nanofiller) and the matrix polymer. For example, the elastic modulus of the aforementioned LDPE/CaCO$_3$ nanocomposite equals approximately 85 MPa [104], and that of the nanofiller amounts to tens of GPa [96], i.e., the difference is over two orders of magnitude. Evidently, deformation of calcium carbonate under such conditions is practically zero, whereas the behavior of the nanocomposite in mechanical tests depends on the behavior of the polymeric matrix [99].

It has recently been proposed to regard the structure of amorphous polymers as a natural nanocomposite [105, 106]. Specifically, it has been supposed in the framework of the cluster model that the amorphous polymer structure consists of local-order regions (clusters) embedded into a loosely packed matrix in which the whole free volume of the polymer is concentrated [65, 94]. The clusters, in turn, consist of a few collinear densely packed statistical segments of various macromolecules, i.e., they are amorphous analogs of extended-chain crystallites. It was shown in books [5, 6] that clusters represent objects of the nanoworld (true nanoparticles or nanoclusters), and when polymers are represented as natural nanocomposites, the clusters play the role of nanofillers, while a loosely packed matrix serves as the nanocomposite matrix. Characteristically, the nanocluster dimension effect is identical with that of disperse nanofillers in polymer nanocomposites: a decrease in the size of both nanoclusters [105] and disperse nanoparticles [97] results in a sharp increase in the reinforcement degree (elastic modulus) of the nanocomposite. These observations pose questions, viz. how does the introduction of a disperse nanofiller influence the size of nanoclusters, and how do its variations influence the elastic modulus of the nanocomposite? The authors of Ref. [107] searched for the answers using an LDPE/CaCO$_3$ nanocomposite [104] as an example.

The answer to the first question comes from determining the number n_{cl} of statistical segments per cluster and its variation with changes in the CaCO$_3$ content. Calculation of n_{cl} includes the following stages. First, the fractal dimension d_f of the nanocomposite structure was found from Eqn (48), then the fraction φ_{cl} of nanoclusters was estimated using the expression [94]

$$d_f = 3-6\left(\frac{\varphi_{cl}}{C_\infty S}\right)^{1/2}, \qquad (62)$$

where the characteristic relation C_∞ is derived in accordance with Eqn (51), and the cross section area S for LDPE particles is assumed to be 14.9 Å^2 [108]. The cluster network density ν_{cl} of macromolecular entanglements can be calculated as [94]

$$\nu_{cl} = \frac{\varphi_{cl}}{C_\infty l_0 S}, \qquad (63)$$

where l_0 is the length of the skeletal bond in the main chain, equaling 1.54 Å for polyethylenes [67].

Thereafter, the molecular mass M_{cl} of the chain segment between nanoclusters was determined in accordance with the equation [94]

$$M_{cl} = \frac{\rho_{pol} N_A}{\nu_{cl}}, \qquad (64)$$

where ρ_{pol} is the polymer density for the LDPE composite, equaling 930 kg m^{-3} [102], and N_A is the Avogadro constant.

Finally, quantity n_{cl} was found from the formula [94]

$$n_{cl} = \frac{2M_e}{M_{cl}}, \qquad (65)$$

where M_e is the molecular mass of the chain segment enclosed between traditional linkage nodes (macromolecular 'overlaps'), equal to 1390 g mol^{-1} for LDPE [66].

Figure 13 plots the dependence of LDPE/CaCO$_3$ elastic modulus E_n on n_{cl}, which reveals a rise in E_n with decreasing n_{cl}. Such a behavior of LDPE/CaCO$_3$ nanocomposites is identical with that of natural nanocomposites [105, 106, 109, 110].

Reference [111] reports the theoretical dependence of E_n on the parameters of a cluster model for natural nanocomposites:

$$E_n = c\,\frac{\varphi_{cl}\nu_{cl}}{n_{cl}}, \qquad (66)$$

where c is a constant assumed to be 1.15×10^{-26} m^3 for the LDPE nanocomposite.

Figure 13 also presents the theoretical dependence $E_n(n_{cl})$ calculated from Eqn (66) for the nanocomposites under consideration, which is in good agreement with experiment (the discrepancy between theory and experiment averages ~ 15% and is comparable with the experimental error in mechanical tests). Thus, increasing the mass content W_n of CaCO$_3$ within a range of 0–50 mass % results in a decrease in

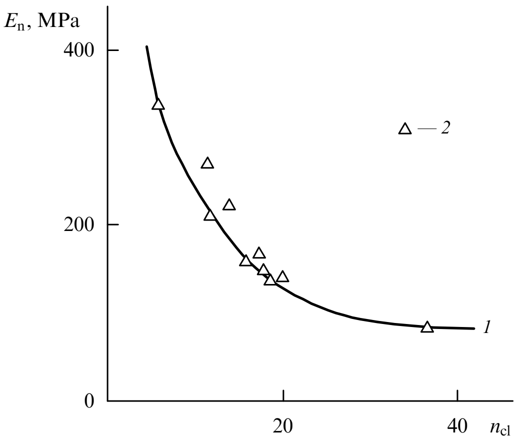

Figure 13. Dependences of elastic modulus E_n on the number n_{cl} of statistical segments per nanocluster in LDPE/CaCO$_3$ nanocomposites: *1* — calculation in accordance with Eqn (66), and *2* — experimental data [107].

$n_{\rm cl}$ from 36.0 to 5.2, and the accompanying growth of LDPE/$CaCO_3$ elastic modulus $E_{\rm n}$ from 85 to 340 MPa.

Let us consider the physical basis behind a decrease in the parameter $n_{\rm cl}$ with increasing nanofiller content in LDPE/$CaCO_3$ nanocomposites. As was shown in Ref. [112], the maximum fraction $\varphi_{\rm pack}$ of densely packed polymer regions is given by the following percolation relation in a thermal cluster model:

$$\varphi_{\rm pack} = \left(\frac{T_{\rm m} - T}{T_{\rm m}}\right)^{\beta_{\rm T}} , \tag{67}$$

where $T_{\rm m}$ and T are the melting and test temperatures, respectively (for LDPE, $T_{\rm m} = 398$ K [102], and $T = 293$ K), and $\beta_{\rm T}$ is the order parameter of a thermal cluster, equal to 0.55 for polymers [113].

Evidently, filling the matrix polymer space with a nanofiller, especially to a high content (up to 50 mass %), decreases the volume fraction of the polymer matrix in the nanocomposite structure. Therefore, the reduced quantity $\varphi_{\rm pack}$ ($\varphi_{\rm pack}^{\rm red}$), defined as [5]

$$\varphi_{\rm pack}^{\rm red} = \frac{\varphi_{\rm pack}}{1 - \varphi_{\rm n}} , \tag{68}$$

needs to be used.

The following sum should be assumed to represent densely packed regions of the nanocomposite structure [5]:

$$\varphi_{\rm pack} = (1 - K)\,\varphi_{\rm cl} + \varphi_{\rm int} , \tag{69}$$

where K is the degree of crystallinity, and $\varphi_{\rm cl}$ and $\varphi_{\rm int}$ are volume fractions of nanoclusters and interfacial regions, respectively.

The $\varphi_{\rm int}$ can be evaluated using the percolation relation (21). Figure 14a plots dependences $\varphi_{\rm pack}^{\rm red}(W_{\rm n})$ for LDPE/$CaCO_3$ nanocomposites. It can be seen that $\varphi_{\rm pack}^{\rm red}$ values determined in accordance with Eqns (67)–(69) are in excellent agreement. Equation (68) gives cause for the decrease in $n_{\rm cl}$ with increasing $W_{\rm n}$ (or $\varphi_{\rm n}$): the reduced fraction of the polymer matrix, together with the decreased in parallel $\varphi_{\rm cl}$, are responsible for the lowered $\nu_{\rm cl}$ value in accordance with Eqn (63), increased $M_{\rm cl}$ in accordance with Eqn (64), and decreased $n_{\rm cl}$ in accordance with Eqn (65).

As expected, constant c in Eqn (66) is a function of matrix polymer characteristics. Figure 14b depicts the dependence of constant c on the elastic modulus $E_{\rm m}$ of matrix polymer for two LDPE species, polypropylene (PP) and polycarbonate (PC). It can be seen that c grows as $E_{\rm m}$ increases and is described by the empirical expression [107]

$$c = 9.71 \times 10^{-26} E_{\rm m} , \tag{70}$$

where $E_{\rm m}$ is given in GPa.

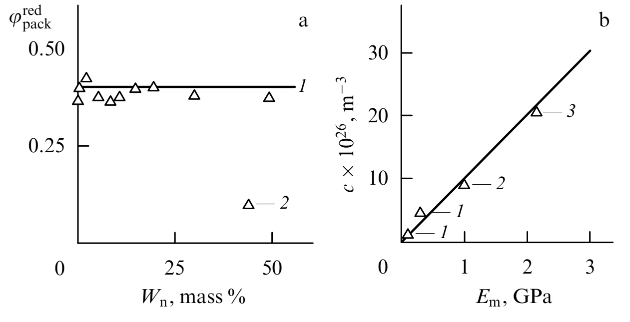

Figure 14. (a) Theoretical dependences of reduced volume fraction $\varphi_{\rm pack}^{\rm red}$ of densely packed regions on nanofiller mass content $W_{\rm n}$ for LDPE/$CaCO_3$ nanocomposites, calculated using Eqns (67), (68) (*1*), and (69) (*2*). (b) Dependence of constant c in Eqn (66) on matrix polymer elastic modulus $E_{\rm m}$ for LDPE (*1*), PP (*2*), and PC (*3*). (Taken from Ref. [107]).

To sum up, the above results demonstrate the general reinforcement mechanism in natural and artificial (containing inorganic nanofiller) polymer nanocomposites that consists in reducing the number of statistical segments per nanocluster with increasing nanofiller content. The physical basis of this effect is the decrease in the polymer matrix volume fraction in the nanocomposite structure upon increasing the amount of the nanofiller.

3.2 Yielding

The yield process characterized in the first place by the yield stress $\sigma_{\rm y}$ attracts great attention from researchers interested in the physics of polymer materials [114] due to the fact that stress $\sigma_{\rm y}$ of plastic polymer materials determines the upper bound of their application range. It accounts for striking differences in the behavior of these materials above and below the yield stress. In the latter case, a material loses its shape as the stress grows, i.e., resists deformation, while in the former one the same effect is observed at a constant stress that is even lower than the yield point (in the presence of a 'fluidity tooth'), due to which this part of the stress–strain curve is frequently referred to as the cold flow. For fragile materials, the upper bound of their application range constitutes the fracture stress. For plastic polymers, the fracture stress is several-fold higher than the yield stress, and this criterion becomes inapplicable. Therefore, yield stress is used as the upper (even if arbitrary) bound of the application range of plastic polymer materials. As is well known, a certain 'reliability factor' lowering the upper bound is used in engineering practice.

There is an opinion [115] assuming that $\sigma_{\rm y}$ is proportional to the modulus of elasticity E. However, later studies (see, e.g., Refs [5, 24]) demonstrated that it is not true in all cases. The proportionality of $\sigma_{\rm y}$ and E does occur in particulate-filled polymer nanocomposites with a glassy amorphous matrix having a stable structure identical with the structure of the matrix polymer [5]. In contrast, it is absent in particulate-filled polymer microcomposites in which the structure of the polymer matrix changes with variation of the filler content [24, 25]. This situation can be accounted for by the following fundamental fact: due to departure from thermodynamically equilibrium structure of polymers in general, and of the composite polymer matrix in particular, a physically correct description of any of their properties requires at least two order parameters [94]. In general, no proportionality between $\sigma_{\rm y}$ and E can be observed for calcium carbonate-filled polymer nanocomposites. Indeed, a rise in the nanofiller content in PP/$CaCO_3$ nanocomposites from 0 to 40 mass % results in a 1.5-fold increase in the modulus of elasticity, whereas $\sigma_{\rm y}$ increases only by 10% [87]. The authors of Ref. [116] considered the structural basis of yield stress variations in LDPE/$CaCO_3$ nanocomposites as an example.

The LDPE/$CaCO_3$ nanocomposites in question are characterized by an even greater difference between the magnitude of changes in elastic modulus $E_{\rm n}$ and yield stress $\sigma_{\rm y}$; specifically, $E_{\rm n}$ increases roughly 4-fold as the $CaCO_3$ content grows from 0 to 50 mass %, whereas yield stress

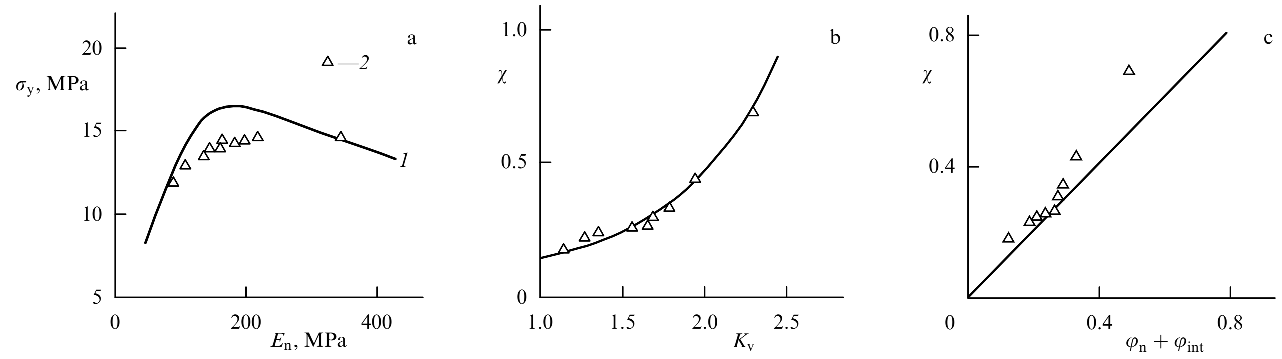

Figure 15. (a) Comparison of theoretical [equation (72)] (*1*) and experimental (*2*) correlations between yield stress σ_y and elastic modulus E_n for LDPE/CaCO$_3$ nanocomposites. (b) Dependence of elastically deformable fraction χ of the structure on stress concentration coefficient K_v for LDPE/CaCO$_3$ nanocomposites. (c) Relationship between elastically deformable fraction χ of the structure and total relative fraction $(\varphi_n + \varphi_{int})$ of nanofiller and interfacial regions for LDPE/CaCO$_3$ nanocomposites. The straight line corresponds to a 1:1 ratio. (Taken from Ref. [116]).

increases only by 23%. The authors of Ref. [116] explained this discrepancy based on the fractal concept of the fluidity process [117], which implies its realization in separate portions of the material rather than in the entire volume. In this case, the Poisson's ratio ν_y at the yield point, i.e., when σ_y is reached, can be estimated as]117]

$$\nu_y = \nu\chi + 0.5(1-\chi)\,, \tag{71}$$

where ν is the Poisson's ratio in the elastic strain region, and χ is the relative fraction of the elastically deformable material.

Assuming $\nu_y = \text{const} = 0.43$ [118] leads to a change in χ from 0.184 to 0.70 associated with the rise in W_n mass content of CaCO$_3$ from 1 to 50 mass %. The quantitative estimation of the yield stress σ_y is possible based on the equation [94]

$$\sigma_y = \frac{\sqrt{3}E_n b_B (\rho_d)^{1/2}}{4\pi(1+\nu)}\,, \tag{72}$$

where b_B is the Burgers vector, ρ_d is the density of linear defects in the structure (analog of dislocations), and ν is the Poisson's ratio.

The values of b_B and ν are calculated in accordance with formulas (50) and (49), respectively. Finally, ρ_d can be defined as [94]

$$\rho_d = \frac{1-\chi}{S}\,, \tag{73}$$

where S is the cross section area of a macromolecule, equaling 14.9 Å^2 for polyethylenes [102].

Figure 15a compares experimental and theoretical [calculation in accordance with Eqn (72)] correlations of $\sigma_y(E_n)$ for LDPE/CaCO$_3$ nanocomposites. It demonstrates excellent agreement between theory and experiment, with the discrepancy between the two averaging $\sim$ 11.6% (comparable with the error of mechanical tests).

Let us consider the physical basis of such a small increase in σ_y for the nanocomposites of interest. It follows from Eqn (72) that a significant increase in E_n is compensated for by the respective decrease in b_B and ρ_d [or $(1-\chi)$]. It can be speculated that a decrease of $(1-\chi)$ or an increase of (χ) is due to a change of the nanocomposite structure after the introduction of the nanofiller. The magnitude of this change can be estimated using the stress concentration coefficient K_v [119] defined by equation (55).

Figure 15b plots the K_v dependence of the elastically strainable structure fraction χ for LDPE/CaCO$_3$ nanocomposites. As expected, χ grows or $(1-\chi)$ decreases with increasing K_v or the degree of nanocomposite structure alteration in comparison with the matrix polymer.

Figure 15c illustrates the relationship between χ and the sum $(\varphi_n + \varphi_{int})$ calculated in accordance with Eqn (21) for the same nanocomposites. Clearly, the structural characteristics χ and $(\varphi_n + \varphi_{int})$ are roughly similar, which suggests that plastic deformation can be realized only in the polymer matrix [116].

The dispersion strength theory [91] provides one more explanation for the very slight increase in σ_y in particulate-filled polymer nanocomposites with an amorphous-crystalline matrix. It follows from Eqns (44), (45), and (47) that a rise in E_n for the nanocomposites being considered is compensated for by an increase in d_f and a decrease in b_B, although the main contribution to this effect comes from $k(r)$. For example, in the absence of aggregation of the initial nanofiller particles, λ decreases from 201 to 9.7 nm as W_n increases within a range from 1 to 50 mass %. The aggregation of these particles in an LDPE/CaCO$_3$ nanocomposite [89] (see also Section 6) leads to a much slighter decrease of $k(r)\,\lambda$ in the above W_n range from 438 to 226 nm.

It is then possible to calculate the theoretically attainable σ_y value for the nanocomposites under consideration in the absence of aggregation of initial filler particles: σ_y will equal 46.3 and 81.9 MPa according to Eqns (72) and (44), respectively. In both cases, it is much higher than in experiment ($\sigma_y = 14.8$ MPa).

Consequently, we may conclude that the introduction of a disperse nanofiller into a polymer amorphous-crystalline matrix markedly alters its structure in comparison with a matrix polymer. The change consists in diminishing the fraction of nanocomposite structure in which plastic deformation is attained. In the end, it results in a weak increase in the yield stress that is not proportional to the elastic modulus, with the growth of nanofiller content. The main factor responsible for this effect is the aggregation of initial nanofiller particles. It has been revealed that yield stress can be significantly increased by suppressing aggregation.

3.3 Failure

It is well known [120] that embrittlement represents one of the main unwanted properties of polymer composites. As a rule, a rise in the nanofiller content impairs composite plasticity, as is apparent from lowered ultimate strain or impact toughness. However, this general tendency does not hold for nanocomposites. For example, the plasticity of particulate-filled polymer nanocomposites [86, 121] and carbon tube-filled nanocomposites [122, 123] increases considerably with a rise in the nanofiller content. This motivated the authors of Ref. [124] to develop a fractal model for the quantitative description of enhanced plasticity (strain to failure) of particulate-filled poly(vinyl) chloride/calcium carbonate (PVC/$CaCO_3$) nanocomposites prepared by *in situ* polymerization [86].

Tensile testing of PVC/$CaCO_3$ nanocomposite samples revealed an extreme enhancement of their plasticity characterized by ultimate strain $\varepsilon_{\rm f}$ with increasing $\varphi_{\rm n}$ (Fig. 16a). The limiting draw ratio $\lambda_{\rm f}$ ($\lambda_{\rm f} = 1 + \varepsilon_{\rm f}$) of polymer materials is estimated by fractal analysis in accordance with the relationship [125]

$$\lambda_{\rm f} = C_{\infty}^{D_{\rm ch}-1}\,, \tag{74}$$

where C_∞ is the characteristic ratio, and $D_{\rm ch}$ is the fractal dimension of the chain segment between its fixation points.

The value of C_∞ was evaluated from Eqn (51), and dimension $D_{\rm ch}$ from the relationship [94]

$$D_{\rm ch} = \frac{\ln n_{\rm st}}{\ln(4 - d_{\rm f}) - \ln(3 - d_{\rm f})}\,, \tag{75}$$

where $n_{\rm st}$ is the number of statistical segments over the chain segment between the clusters, calculated from the formula [94]

$$n_{\rm st} = \frac{1}{\varphi_{\rm cl}}\,. \tag{76}$$

Figure 16a compares theoretical [calculated from Eqn (74)] and experimental ultimate strains $\varepsilon_{\rm f}$ as a function of $CaCO_3$ content $\varphi_{\rm n}$ for PVC/$CaCO_3$ nanocomposites. The two parameters are in excellent qualitative and good enough quantitative agreement, with the discrepancy between experimental and calculated $\varepsilon_{\rm f}$ values averaging $\sim 16\%$. In other words, equations (48), (49), (51), and (74)–(76) give a clear physical picture of the enhanced plasticity of PVC/$CaCO_3$ nanocomposites. This effect is due to the increase in the elastic modulus $E_{\rm n}$ of nanocomposites with increasing $\varphi_{\rm n}$ in the range from 0 to 0.050 and its subsequent decrease at $\varphi_{\rm n} = 0.075$ associated with the aggregation of $CaCO_3$ nanoparticles that results in an extreme $d_{\rm f}(\varphi_{\rm n})$ dependence in accordance with Eqns (48) and (49). Dimension $d_{\rm f}$ being the principal structural characteristic of a nanocomposite that determines its main structural parameters [see Eqns (51), (62), and (75)], the behavior of $d_{\rm f}$ ultimately determines any modification of nanocomposite properties including $\varepsilon_{\rm f}$ [124].

The dependence $\varepsilon_{\rm f}(d_{\rm f})$ presented in Fig. 16b indicates that $\varepsilon_{\rm f} = 0$ at $d_{\rm f} \approx 2.66$, i.e., an ideally brittle failure of PVC/$CaCO_3$ nanocomposites takes place. This means that the failure of these nanocomposites in the $d_{\rm f} \leqslant 2.66$ range largely occurs through cracking at all stages of this process [75]. Extrapolation of the linear dependence $\varepsilon_{\rm f}(d_{\rm f})$ to the maximum value of $d_{\rm f} = 2.95$ for real solids [75] gives the maximum ultimate strain $\varepsilon_{\rm f}^{\rm max} = 1.28$ for the nanocomposites being considered.

Thus, the above results indicate that a variation of plasticity in PVC/$CaCO_3$ nanocomposites (an extreme increase with $\varphi_{\rm n}$) is due to a similar change in the elastic modulus, with the yield stress remaining roughly constant. This effect can be described in quantitative terms in the framework of fractal analysis. The reduction in the modulus of elasticity caused by aggregation of nanofiller particles upon an increase in their content accounts for the impaired plasticity of nanocomposites.

The authors of Refs [121, 126] revealed that the introduction of a disperse nanofiller $CaCO_3$ into high-density polyethylene (HDPE) increases the impact toughness $A_{\rm p}$ of HDPE/$CaCO_3$ nanocomposites by approximately 20% over that of the parent polymer. Detailed fractographic analysis of this effect in Refs [121, 126] provided an explanation for the observed enhancement of $A_{\rm p}$ as being due to a change in the plastic deformation mechanism in HDPE/$CaCO_3$ nanocomposites compared with that in the original HDPE polymer. It should be noted, without going into the particulars of this analysis, that its correctness is open to question.

Figure 17 presents load vs time ($P-t$) schematic diagrams illustrating two cases of the failure of polymer materials by unstable (a) and stable (b) cracks in instrumental impact tests. The quantity $A_{\rm p}$ is known to be characterized by the area under the $P-t$ curve, giving the mechanical energy needed to destroy the samples [127]. The macroscopic failure process in polymer materials caused by the main crack propagation originates at a maximum load P. It follows from the $P-t$ diagrams that the failure process proper hardly affects $A_{\rm p}$ in the case of unstable crack propagation and only slightly

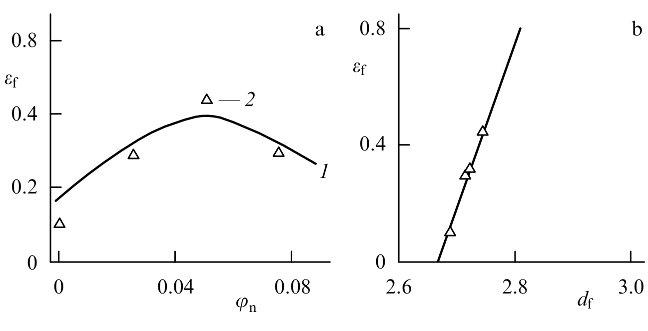

Figure 16. (a) Dependences of calculated from Eqn (74) (*1*) and experimental (*2*) ultimate strain $\varepsilon_{\rm f}$ on nanofiller content $\varphi_{\rm n}$ for PVC/$CaCO_3$ nanocomposites. (b) Dependence of ultimate strain $\varepsilon_{\rm f}$ on structure fractal dimension $d_{\rm f}$ for PVC/$CaCO_3$ nanocomposites. (Taken from Ref. [124]).

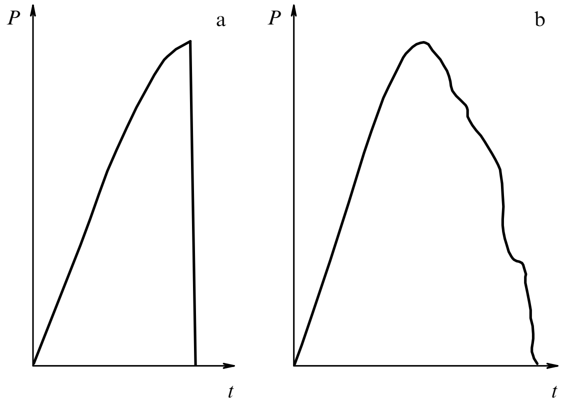

Figure 17. Schematic of load vs time ($P-t$) diagrams illustrating destruction by unstable (a) and stable (b) cracks in instrumental impact tests [129].

affects it in the case of a stable crack. The authors of Refs [121, 126] performed instrumental impact tests, allowing them to obtain $P-t$ diagrams, but did not present them in their articles.

Moreover, the structural aspect of the failure process was considered in Refs [121, 126] with the use of secondary structures (shift zones, crazes, etc.). Their relationship with the structure of the starting intact material is purely speculative. Evidently, this analytical method does not permit obtaining the quantitative structure–property relationships (which is the main task in polymer physics) [128]. Therefore, the authors of Refs [129, 130] performed the quantitative structural analysis of the results of impact tests of HDPE polymers and HDPE/$CaCO_3$ nanocomposites in the framework of fractal models.

As is well known [131], fractal dimension d_f carries most general structural information about an object (in our case — a polymer). Indeed, it is a true structural characteristic describing the spatial arrangement of structure elements. It can be determined according to Eqn (62) in which parameter φ_{cl} is estimated from the following percolation relation [113]:

$$\varphi_{cl} = 0.03(1 - K)(T_m - T)^{0.55}\,, \qquad (77)$$

where K is the degree of crystallinity, equaling 0.48 and 0.55 for the parent HDPE and the HDPE/$CaCO_3$ nanocomposite (containing 5 mass % of the nanofiller), respectively [126], T_m is the melting temperature of these materials ($\sim$ 406 K) [126], and T is the test temperature.

To recall, the value of d_f calculated from Eqn (62) agrees with those obtained by other methods. For example, it can be calculated using an alternative equation (48). The values of d_f, in accordance with Eqns (62) and (48), are 2.73 and 2.68, respectively, for HDPE, compared with 2.75 and 2.73 for the HDPE/$CaCO_3$ nanocomposite. Clearly, these estimates are in excellent agreement: the discrepancy between the fractional parts of d_f carrying the main structural information does not exceed 7%.

Figure 18a plots the $A_p(d_f)$ dependence for these polymer materials that proved to be linear an common to the parent HDPE and the HDPE/$CaCO_3$ nanocomposite. This dependence is described by the following empirical correlation [129]:

$$A_p = 13.5(d_f - 2.5)\ [\text{kJ m}^{-2}]\,. \qquad (78)$$

It follows from the last expression that $A_p = 0$ at $d_f = 2.5$. This fractal dimension corresponds to the ideal brittle failure condition [75] that leads to the condition $A_p = 0$. The maximum fractal dimension of the structure of real solids amounts to 2.95 [75], which makes it possible to determine the maximum A_p value from formula (78) as equaling ~ 6.1 kJ m^{-2}.

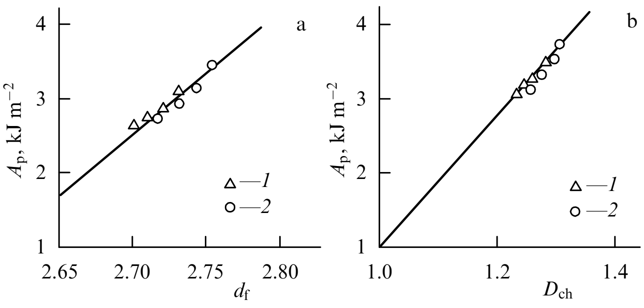

Figure 18. (a) Impact toughness A_p vs structure fractal dimension d_f for HDPE polymer (*1*) and HDPE/$CaCO_3$ nanocomposite (*2*) [129]. (b) Impact toughness A_p vs fractal dimension D_{ch} of intercluster chain segment for HDPE polymer (*1*) and HDPE/$CaCO_3$ nanocomposite (*2*) [130].

It was shown by Kausch [132] that energy dissipation induced by an impact increases with increasing molecular mobility in a polymer material. In the framework of fractal analysis, the level of this mobility can be characterized by fractal dimension D_{ch} of the polymer chain segment between its fixation points [94]. This analytical method was successfully used in describing quantity A_p for particulate-filled phenylone/β-sialon nanocomposites [133]. The value of D_{ch} can be found from Eqn (75).

Figure 18b depicts the dependence of impact toughness A_p on fractal dimension D_{ch} for the above materials. As expected, A_p grows as D_{ch} increases; this interplay is analytically described by the relation [130]

$$A_p = 6.75(D_{ch} - 1)\ [\text{kJ m}^{-2}]\,. \qquad (79)$$

The last equation allows the maximum A_p value for the materials of interest to be determined as 6.75 kJ m^{-2} at $D_{ch} = 2.0$. This estimate is close to that obtained above from Eqn (78), the discrepancy being, on average, less than 10%.

Let us consider conditions for attaining zero impact toughness at $d_f = 2.5$ but not at $d_f = 2.0$ ($2.0 \leqslant d_f < 3.0$) [75]. As is well known [134], the structure of any polymer, including HDPE, reaches quasiequilibrium state when the growth of φ_{cl}, regardless of its cause, becomes balanced by entropic tension of polymer chains and stops. Reference [134] reports that the structural dimension of the HDPE quasiequilibrium state is equal to ~ 2.50. Calculation according to Eqn (75) indicates that, in this case, $D_{ch} \approx 1.0$, which means that the polymer material becomes ideally brittle.

Equations (78) and (79) allow estimating the theoretical values of impact toughness A_p^{theor} and comparing them with experimental A_p. Such a comparison is drawn in Fig. 19, showing good agreement between theory and experiment. The discrepancy between A_p^{theor} and A_p averages 3.5% and 3.9% if Eqns (78) and (79) are used, respectively, for the calculations. These values are significantly lower than the routine experimental error amounting to $\sim$ 10% when impact toughness is determined.

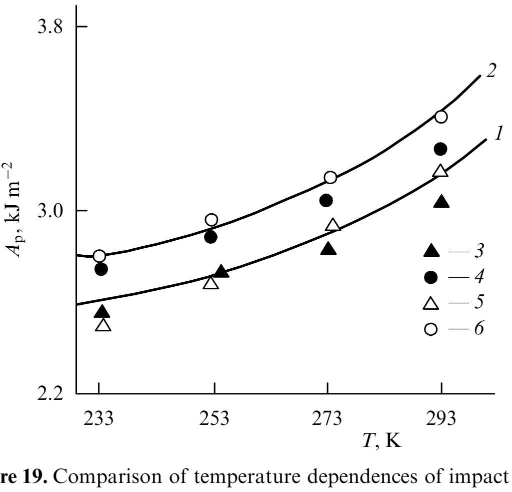

Figure 19. Comparison of temperature dependences of impact toughness A_p: experimental (*1*, *2*) and calculated from Eqns (78) (*3*, *4*) and (79) (*5*, *6*) for HDPE polymer (*1*, *3*, *5*) and HDPE/$CaCO_3$ nanocomposite (*2*, *4*, *6*) [130].

Let us consider the physical basis of the impact toughness enhancement for HDPE/$CaCO_3$ nanocomposites in comparison with the matrix polymer HDPE. The plots in Fig. 18a, b give evidence that a rise in A_p is due to increased d_f and D_{ch} dimensions, respectively. At the same time, it follows from Eqns (62) and (75) that an increase in these dimensions is related to decreased φ_{cl}, because the molecular characteristics C_∞ and S are assumed to be constant. It follows from Eqn (77) that a decrease in φ_{cl} depends only on the increase in the degree of crystallinity K, since quantity T_m is practically identical for HDPE polymer and HDPE/$CaCO_3$ nanocomposite. This means that an increase in A_p for the HDPE/$CaCO_3$ nanocomposite, as opposed to that for the matrix polymer HDPE, is due to the action of $CaCO_3$ as a nucleator promoting the growth of K [121, 126].

It follows from the foregoing that fractal analysis makes it possible to construct a quantitative impact toughness model for high-density polyethylene and a particulate-filled nanocomposite containing HDPE, taking account of the structural characteristics of these materials. The increase in impact toughness is due to the action of the nanofiller as a nucleator of crystallization and the resulting alteration of the amorphous phase structure. Calculations revealed excellent agreement between theory and experiment.

3.4 Microhardness

As is well known [135–137], microhardness H_B specifies a property sensitive to morphological and structural changes in polymer materials. An additional important factor for nanocomposite materials is the presence of a filler whose microhardness is much higher than that of the polymer matrix [138]. After sharp-pointed (conical or pyramidal) indenters are introduced into a polymer, the stress becomes localized within a rather small microvolume. Such testing is supposed to help a researcher to 'grope his/her way' towards the real structure of polymer materials [139]. The complex structure of polymer nanocomposites [5] poses the question of what structural component responds to indentation and how its reaction changes after a disperse nanofiller is introduced.

Another aspect of the problem is the relationship between microhardness determined by testing in a strongly localized microvolume and such macroscopic properties of polymer materials as elastic modulus E and yield stress σ_y. At present, there are many theoretically and empirically derived relationships among H_B, E, and σ_y [140, 141]. The authors of Ref. [142] described microhardness in terms of fractal analysis and elucidated its relationship with the structure of HDPE/$CaCO_3$ nanocomposites as an example [143, 144].

Let us consider the relationship between microhardness H_B and other mechanical characteristics, such as yield stress σ_y for HDPE/$CaCO_3$ nanocomposites [143, 144]. Tabor [145] derived the following relation between H_B and σ_y for metals regarded as hard, perfectly plastic solids:

$$\frac{H_B}{\sigma_y} \approx c\,, \tag{80}$$

where c is a constant roughly equal to 3.

Relation (80) suggests that pressure under the indenter applied in microhardness tests is higher than the yield stress in quasistatic tests due to constraints imposed by the unstrained polymer surrounding the indenter. However, a number of authors [137, 140, 141, 143, 146] demonstrated that the c value may be significantly different than 3 and vary in a fairly wide range of $\sim 1.5-30$. It was revealed in Ref. [143] that in HDPE/$CaCO_3$ nanocomposites c varies from 1.80 to 5.83, depending on the strain rate $\dot{\varepsilon}$ and the type of quasistatic tests for determining σ_y (stretching or compression). The H_B/σ_y ratio approaches $c = 3$ only in the case of a minimal $\dot{\varepsilon}$ and the use of σ_y values obtained in compression tests. Based on these findings, the authors of Ref. [143] concluded that the value of $c = 3$ can be reached only at comparable strain rates in microhardness tests and in quasistatic tests in the presence of intact polymer–filler interfaces.

To extend the analysis to a wider circle of solids, it was proposed to consider the role of elasticity in indentation. The following equation was derived for a solid with elastic modulus E and Poisson's ratio ν [140]:

$$H_B = \frac{2}{3}\left[1 + \ln\frac{E}{3(1-\nu)\,\sigma_y}\right]\sigma_y\,, \tag{81}$$

with the empirical Marsh equation having the form [140]

$$H_B = \left(0.07 + 0.6\,\ln\frac{E}{\sigma_y}\right)\sigma_y\,. \tag{82}$$

Equations (81) and (82) allow the H_B/σ_y ratio for HDPE/$CaCO_3$ nanocomposites to be estimated [144] provided quantities E and σ_y are known, while ν can be calculated using relation (49).

Figure 20a presents the dependences of H_B/σ_y on the strain rate $\dot{\varepsilon}$ calculated from equations (81) and (82) for the HDPE polymer and HDPE/$CaCO_3$ nanocomposites with $CaCO_3$ particles 70 nm in size [144]. Notice that in this case σ_y values are obtained in tensile tests. Evidently, equations (81) and (82) give H_B/σ_y values close to 3 for both the parent HDPE and the HDPE/$CaCO_3$ nanocomposite with a $CaCO_3$ content $\varphi_n = 0.10$ [deviation of the calculated H_B/σ_y from $c = 3$ is less than 10%, in excellent agreement with the approximate character of Eqn (80)].

Let us consider the physical nature of H_B/σ_y deviation from constant $c \approx 3$ in Eqn (80) using the Marsh relationship (82) as the simplest one. As is well known [75], the fractal dimension d_f of the nanocomposite structure can be calculated from Eqn (48). Combining formulas (48), (49), and (82) leads to the following relation [142]

$$\frac{H_B}{\sigma_y} = 0.07 + 0.6\,\ln\frac{3d_f}{3-d_f}\,. \tag{83}$$

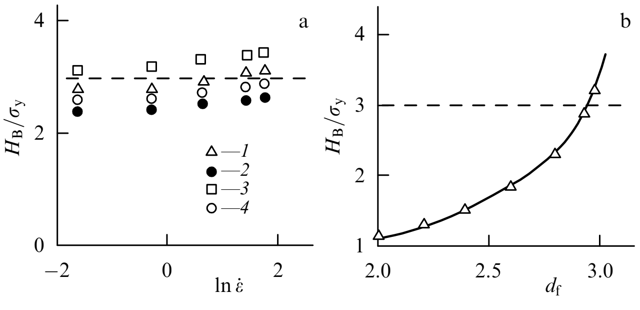

Figure 20. (a) Dependences of H_B/σ_y ratio calculated in accordance with Eqns (81) (*1*, *3*) and (82) (*2*, *4*) on strain rate $\dot{\varepsilon}$ in logarithmic coordinates for HDPE (*1*, *2*) polymer and HDPE/$CaCO_3$ nanocomposite (*3*, *4*). (b) Dependence of H_B/σ_y ratio on structure fractal dimension d_f calculated in accordance with Eqn (83). Horizontal dashed line indicates Tabor's criterion $H_B/\sigma_y = c \approx 3$. (Taken from Ref. [142].)

It ensues from the last relation that the H_B/σ_y ratio is only determined by fractal dimension d_f. Figure 20b demonstrates the dependence of H_B/σ_y on d_f, suggesting that the value of $H_B/\sigma_y = c \approx 3$ is reached at $d_f \approx 2.93$. To recall, the value of d_f for real solids cannot be higher than 2.95 [75]. In other words, the equality $c \approx 3$ in Eqn (80) is only fulfilled for Euclidean (or close to Euclidean) bodies having a dimension approaching 2.95. Calculations using Eqns (48) and (49) showed that d_f for HDPE/CaCO$_3$ nanocomposites varies from 2.878 to 2.920, which explains the closeness of the ratio H_B/σ_y to 3 in these materials (Fig. 20a). For phenylone/silicon–yttrium oxynitride nanocomposites, one has $d_f = 2.42$ [147], which gives $H_B/\sigma_y \approx 1.60$, in accordance with Eqn (83). This value is consistent with the H_B/σ_y ratio of ≈ 2 for these nanocomposites, obtained in experiment [146]. This line of reasoning makes it clear why Tabor obtained the value of $c \approx 3$ just for metals that are actually Euclidean objects [75].

To sum up, the above results indicated that the microhardness/yield stress ratio for polymer materials only depends on their structural state characterized by a fractal dimension. The constant in Tabor's equation equals 3 only for solids having a structure that is close to Euclidean.

4. Thermophysical properties

The authors of Ref. [148] considered the synergetic effect of the specific thermal conductivity of hybrid nanocomposites based on amorphous polyamide (phenylone C-2) and filled with short carbon fibers and a disperse nanofiller. Hybrid composites are usually termed those containing two or more different nanofillers [149]. The authors of Ref. [149] proposed introducing two types of nanofillers, rubber and glass disperse particles, into a brittle epoxy matrix for different functional purposes: the rubber particles enhance the plasticity of the fragile epoxy polymer, while the glass particles increase its hardness. The authors of Ref. [103] proposed a new form of hybrid reinforcement, namely the reinforcement of polyamide-6 with short fibers and organoclay (Na$^+$-montmorillonite), i.e., micro- and nanofiller. The introduction of such fillers considerably enhances both the hardness and the thermal stability of hybrid nanocomposites under study.

In Ref. [148], polymer matrix reinforcement was achieved using uglen-9 carbon fibers with the surface modified by chlorine (UC) and amino groups (UAG). The fiber content was 17 mass %. The refractory ultradisperse silicon–yttrium oxynitride $Si_3N_4-Y_2O_3$ (SYON) powder with a particle size of 80–120 nm, specific surface of 42.5 m^2 g^{-1}, and SYON content of 1 mass % served as disperse nanofiller.

Table 2 lists experimental specific heat conductivities λ_T for matrix phenylone C-2, phenylone/UC and phenylone/UAG microcomposites, the phenylone/SYON nanocomposite, and phenylone/UC-SYON and phenylone/UAG-SYON hybrid nanocomposites containing the aforementioned amounts of UC, UAG, and SYON. Evidently, short fibers and a disperse nanofiller introduced separately cause only a slight (less than 20%) rise in λ_T, whereas the introduction of the hybrid UAG–SYON filler increases phenylone λ_T by 80%. Let us consider this synergetic effect in more detail.

Table 2. Comparison of experimental thermal conductivities λ_T of phenylone-based composites with those (λ_T^{theor}) calculated from Eqns (84) and (85) [148].

Composite	λ_T, W m^{-1} K^{-1}	λ_T^{theor}, W m^{-1} K^{-1}
Phenylone	0.29	—
Phenylone/SYON	0.30	—
Phenylone/UC	0.33	0.34
Phenylone/UAG	0.35	0.34
Phenylone/UC–SYON	0.46	0.50
Phenylone/UAG–SYON	0.52	0.50

In the framework of fractal analysis, a system of filler particles (particle aggregates) is described in terms of the fractal dimension D_B of the filler particle backbone that characterizes the spatial density of polymer matrix filling with particulates or fibers [24, 26]. The fractal model next considers a random mixture of components A and B containing well and poorly conducting portions [150]. This model fully corresponds to polymer composites in which the heat conductivity of the filler and the polymer matrix may differ by three orders of magnitude [151]. Two limiting cases of this problem deserve special attention [150]:

(1) random resistor network (RRN). It is assumed that sites occupied by a poor conductor B have zero conductivity;

(2) random superconductor network (RSN). It is assumed that the conductivity of a good conductor A is infinite.

The authors of Refs [152, 153] demonstrated in the framework of the above general model that the two main cases hold for polymer composites filled with short fibers. For $D_B < 2.62$ (RSN limit), the dependence $\lambda_T(D_B)$ is approximated by the following equation

$$\lambda_T = 0.90(D_B - 2)\ [W\ \text{m}^{-1}\ \text{K}^{-1}]\,; \tag{84}$$

while for $D_B \geqslant 2.62$ (RRN limit), the approximation of $\lambda_T(D_B)$ dependence has the form

$$\lambda_T = 0.51(D_B - 2)\ [\text{W m}^{-1}\ \text{K}^{-1}]\,. \tag{85}$$

Worthy of attention is the fact that the numerical coefficient in Eqn (84) also exceeds by approximately 80% the analogous coefficient in Eqn (85). Such compatibility between the increase in λ_T for hybrid nanocomposites and the same value for composites filled with short fibers alone needs quantitative verification.

Quantity D_B is related to the surface dimension d_0 of initial filler particles (fibers) by Eqn (40), from which the volume fraction of interfacial regions can be determined in the following way. First, the fiber orientation factor η is calculated using the formula [154]

$$\sigma_f^c = \eta \tau_y \frac{\bar{l}}{\bar{d}}\, \varphi_n + \sigma_f^m (1 - \varphi_n)\,, \tag{86}$$

where σ_f^c and σ_f^m are the fracture stress of the composite and the polymer matrix, respectively, τ_y is the yield stress of the polymer matrix in the shearing test, $\bar{l}/\bar{d}$ is the mean fiber length-to-diameter ratio, and φ_n is the volumetric filler content.

Quantities σ_f^c and σ_f^m (σ_f^m is assumed to equal the matrix phenylone toughness) can be found based on the results of mechanical tests (see Fig. 21 as an example), the $\bar{l}/\bar{d}$ ratio for uglen (with a content 17 mass %) is ~ 11 [155], and τ_y is determined from formula (46).

The values of η for the four short fiber-filled composites with and without SYON were estimated using Eqn (86) to be close to 0.145. The quantity φ_{int} can then be determined from the equation [26]

$$\varphi_{\text{int}} = 1.09\eta\,. \tag{87}$$

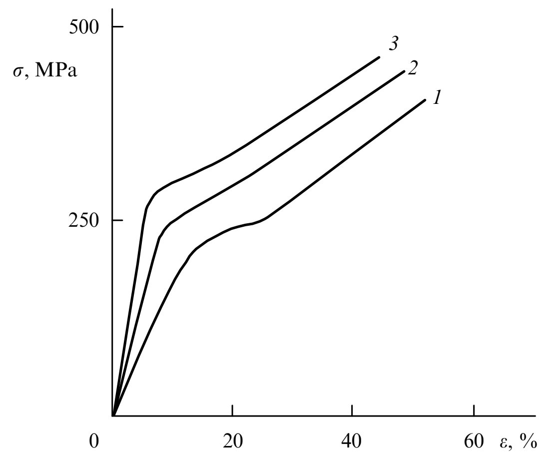

Figure 21. Stress–strain ($\sigma-\varepsilon$) diagrams for uniaxial compression of phenylone (*1*), phenylone/UC–SYON (*2*), and phenylone/UAG–SYON (*3*) hybrid nanocomposites [148].

Next, the estimation of quantity d_0 for relatively smooth uglen-9 fibers yields 2 [26]. Its value for SYON can be calculated using Eqn (7), which gives $d_0 = 2.48-2.52$ (mean 2.50). If $d_0 = 2$ for composites filled with uglen-9 fibers alone (UC or UAG), then d_0 for hybrid nanocomposites can be estimated according to the mixture rule, giving $d_0 = 2.04$ for hybrid fillers UC–SYON and UAG–SYON. Calculations with the use of Eqn (40) then showed that $D_{\rm B} = 2.66$ for phenylone/UC and phenylone/UAG composites, while $D_{\rm B} = 2.56$ for hybrid nanocomposites. It is readily seen that in accordance with the aforementioned classification, $D_{\rm B} > 2.62$ for phenylone/UC and phenylone/UAG microcomposites, which corresponds to the RRN limit [Eqn (85)]. For hybrid nanocomposites, on the contrary, $D_{\rm B} < 2.62$ and they correspond to the RSN limit [Eqn (84)]. The results of a theoretical calculation of thermal conductivity $\lambda_{\rm T}$ ($\lambda_{\rm T}^{\rm theor}$) using the above equations are presented in Table 2, demonstrating their excellent agreement with experimental data (the average discrepancy between $\lambda_{\rm T}$ and $\lambda_{\rm T}^{\rm theor}$ being less than 5%).

Such a substantial increase in $\lambda_{\rm T}$ upon introducing only 1 mass % of SYON is due to the closeness of the $D_{\rm B}$ value for phenylone/UC and phenylone/UAG composites to its boundary value 2.62. Nevertheless, it is possible to vary $D_{\rm B}$ in a wider range, either by increasing disperse nanofiller content or by supplying an alternative nanofiller with a higher d_0.

To conclude, an improvement in the thermophysical properties of polymer composites, including heat conductivity, has important practical implications. Enhanced thermal conductivity markedly improves heat removal from local sources and thereby extends the scope of applications of polymer composites. In other words, the introduction of a hybrid filler substantially increases the traditionally low thermal conductivity of polymers (by approximately two orders of magnitude lower than that in metals) [151]. Characteristically, this effect is realized by virtue of the main property of nanomaterials, i.e., the enlargement of the polymer matrix–filler interface surface after introducing SYON to the matrix [38].

Thus, the above results demonstrated that the introduction of hybrid fillers into polymers gives rise to creating polymer composites with improved working properties, such as enhanced thermal conductivity. The introduction of 1 mass % of a disperse nanofiller produces the same effect as filling with ~ 20 mass % of short fibers. The theoretical explanation of this effect should be looked for in the framework of the fractal concept of random mixture conductivity.

Inorganic nanofillers are also found wide utility in producing polymer nanocomposites [5]. However, the properties of polymer melts for the nanocomposites of interest are insufficiently known. As a rule, the application of nanofillers is a matter of compromise among the improvement in their solid-phase mechanical properties, the enhancement of melt viscosity during treatment, nanofiller dispersion, and cost-effectiveness. In this context, elucidation of the relationship of nanofiller concentration and geometry with nanocomposite melt properties is an important aspect of investigations into the structure of these materials. With this in mind, the authors of Refs [156, 157] undertook research and a theoretical description of the dependence of HDPE/CaCO$_3$ nanocomposite melt viscosity [104] on nanofiller concentration.

Two simple relations among melt viscosity η, shear modulus G in the solid state, and volumetric filling degree $\varphi_{\rm n}$ were obtained for polymer microcomposites, i.e., composites with micrometer-size fillers. The relation between η and G has the form

$$\frac{\eta}{\eta_0} = \frac{G}{G_0}\,, \tag{88}$$

where η_0 and G_0 are the melt viscosity and shear modulus of the matrix polymer, respectively.

Moreover, an increase in microcomposite melt viscosity can be estimated as follows (for $\varphi_{\rm n} < 0.40$) [158]:

$$\frac{\eta}{\eta_0} = 1 + \varphi_{\rm n}\,. \tag{89}$$

Figure 22a plots the dependences of $G_{\rm n}/G_{\rm m}$ amd $\eta_{\rm n}/\eta_{\rm m}$ rations ($G_{\rm n}$ and $\eta_{\rm n}$ are the nanocomposite shear modulus and melt viscosity, while $G_{\rm m}$ and $\eta_{\rm m}$ are the same parameters for the starting matrix polymer) on the CaCO$_3$ mass content $W_{\rm n}$ for HDPE/CaCO$_3$ nanocomposites, where the inverse melt flow index (MFI) is used as a measure of melt viscosity η. The data in Fig. 22a clearly demonstrate that relation (88) is neither qualitatively nor quantitatively fulfilled for the nanocomposites being considered: a drop in the $\eta_{\rm n}/\eta_{\rm m}$ ratio

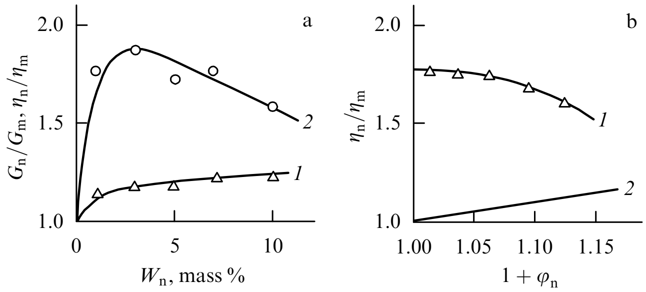

Figure 22. (a) Dependences of the ratios of shear moduli $G_{\rm n}/G_{\rm m}$ (*1*) and melt viscosities $\eta_{\rm n}/\eta_{\rm m}$ (*2*) for nanocomposite ($G_{\rm n}$, $\eta_{\rm n}$) and matrix polymer ($G_{\rm m}$, $\eta_{\rm m}$) on nanofiller mass content $W_{\rm n}$ in HDPE/CaCO$_3$ nanocomposites. (b) Dependence of the ratio $\eta_{\rm n}/\eta_{\rm m}$ of nanocomposite and matrix polymer melt viscosities on volumetric nanofiller content ($1 + \varphi_{\rm n}$) (*1*) for HDPE/CaCO$_3$ nanocomposites. Straight line *2* corresponds to a 1:1 ratio. (Taken from Ref. [157].)

with the growth of W_n corresponds to an increase in $G_{\rm n}/G_{\rm m}$, and the absolute $\eta_{\rm n}/\eta_{\rm m}$ values are much higher than the respective $G_{\rm n}/G_{\rm m}$ values.

Figure 22b compares $\eta_{\rm n}/\eta_{\rm m}$ and $(1+\varphi_{\rm n})$ parameters for HDPE/$CaCO_3$ nanocomposites. Here, experimental data and the results calculated from relation (89) again disagree: there is a discrepancy between the absolute values of $\eta_{\rm n}/\eta_{\rm m}$ and $(1+\varphi_{\rm n})$, and an increased $1+\varphi_{\rm n}$ corresponds to a decreased relative viscosity of the melt. The plot in Fig. 22b was constructed using the nominal value of $\varphi_{\rm n}$ that disregards aggregation of nanofiller particles and can be estimated from Eqns (15) and (37).

Thus, the data of Fig. 22b demonstrate that relationships (88) and (89), satisfiable in the case of polymer microcomposites, are incorrect for nanocomposites. Let us consider this case in more detail. If relation (88) is correct and the Kerner equation is applied to calculate G, the lower viscosity limit $\eta_{\rm n}$ can be found in accordance with the expression [158]

$$\frac{\eta_{\rm n}}{\eta_{\rm m}} = 1 + \frac{2.5\varphi_{\rm n}}{1-\varphi_{\rm n}} \,. \tag{90}$$

Since the quantity η is inversely proportional to MFI, such an interpretation allows Eqn (90) to be rewritten as [157]

$$\frac{\rm MFI_m}{\rm MFI_n} = 1 + \frac{2.5\varphi_{\rm n}}{1-\varphi_{\rm n}} \,, \tag{91}$$

where $\rm MFI_m$ and $\rm MFI_n$ are the MFI values for the matrix polymer and the nanocomposite, respectively.

Three methods are available to estimate $\varphi_{\rm n}$ in Eqns (90) and (91). One (yielding the nominal $\varphi_{\rm n}$ value) was described in the preceding paragraphs. Another is usually employed for microcomposites, when block filler density is used as ρ_0, i.e., $\rho_0 = {\rm const} = 2000$ kg m^{-3} in the case of $CaCO_3$. The third method also makes use of Eqns (15) and (37) but takes account of nanofiller particle aggregation; in this case, the diameter $D_{\rm p}$ of particles of the starting nanofiller in Eqn (15) is substituted by the diameter $D_{\rm ag}$ of their aggregate. The degree of aggregation of $CaCO_3$ nanoparticles and, therefore, $D_{\rm ag}$ can be estimated in the framework of the dispersion toughness theory [91] [see Eqn (52)]. Calculation according to Eqn (52) revealed an increase in $D_{\rm ag}$ (corresponding to that of $k(r)$) from 320 to 580 nm in the range of $W_{\rm n} = 1-10$ mass%. Furthermore, Eqn (15) can be used to calculate the real ρ_0 value for an aggregated nanofiller, and Eqn (37) to evaluate the real volumetric filling degree $\varphi_{\rm n}$.

Figure 23 compares $\rm MFI_n(W_n)$ dependences (experimental and calculated according to formula (91) with tapping the $\varphi_{\rm n}$ values estimated with the help of the above methods). Evidently, there is neither qualitative nor quantitative agreement between theory and experiment.

This disagreement necessitates application of an altogether different approach to the description of polymer nanocomposite melt viscosity, such as fractal analysis, which enabled the authors of Ref. [159] to propose the following relationship for estimating the fractal fluid viscosity η:

$$\eta(l) \sim \eta_0 l^{2-d_{\rm f}} \,, \tag{92}$$

where l is the characteristic linear flow scale, η_0 is a constant, and $d_{\rm f}$ is the fractal dimension.

In the present case, l should be regarded as the radius of an aggregate of $CaCO_3$ particles, $D_{\rm ag}/2$. Because the surface of this aggregate is in contact with the polymer, $D_{\rm f}$ was chosen to be represented by its fractal dimension $d_{\rm s}$ which can be calculated from Eqns (26) and (7). As before, η is considered the inverse quantity of $\rm MFI_n$, and constant η_0 is put equal to $(\rm MFI_m)^{-1}$. Under these conditions and upon the substitution of the equality sign in relation (92) for the proportionality sign the possibility appears for calculating the value of $\rm MFI_n$ if $D_{\rm ag}$ is expressed in micrometers. Figure 23 compares the calculated $\rm MFI_n$ with the measured $\rm MFI_n(W_n)$ values, which suggests excellent agreement between theory and experiment.

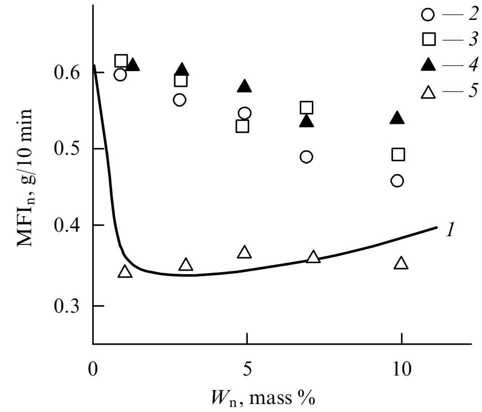

Figure 23. Dependence of melt flow index (MFI) on filler mass content $W_{\rm n}$ for HDPE/$CaCO_3$ nanocomposites: *1* — experimental data; *2–4* — calculation in accordance with Eqn (91) taking (*3*) and not taking (*2*) account of nanofiller particle aggregation and under condition of $\rho_0 = {\rm const}$ (*4*), and *5* — calculation in accordance with Eqn (92) [157].

Relation (92) allows a few conclusions to be drawn. To begin with, an increase in $D_{\rm ag}$, i.e., enhanced aggregation of initial nanoparticles, under the above conditions causes nanocomposite melt viscosity to decrease, while the enhanced nanoparticle surface roughness increases melt viscosity. At $d_{\rm s} = 2.0$, i.e., when nanofiller particles have a smooth surface, the melts of the matrix polymer and the nanocomposite have similar viscosities. Interestingly, extrapolation of the dependence of experimental $\rm MFI_n$ on the $d_{\rm s}$ values calculated from Eqn (7) gives $\rm MFI_n = 0.602$ g/10 min at $d_{\rm s} = 2.0$, which is practically equal to experimental $\rm MFI_n = 0.622$ g/10 min. These factors, critical for nanofillers, are disregarded in the continual interpretation of polymer composite melt viscosity [see Eqn (90)].

Thus, the above results showed that the models developed to describe microcomposite rheological properties do not ensure an adequate interpretation of melt viscosity for particulate-filled polymer nanocomposites. A correct description of nanocomposite rheological properties is possible in the framework of the fractal model of viscous fluid flow. Characteristically, such an approach is essentially different from those employed to describe microcomposites. For example, aggregation of nanofiller particles reduces both melt viscosity and the nanocomposite elastic modulus in the solid state. In contrast, a rise in melt viscosity for microcomposites results in an enhanced modulus of elasticity.

5. Application prospects of particulate-filled polymer nanocomposites

At present, three main types of nanofillers for polymers are distinguished, viz. disperse particles, organoclay, and carbon nanotubes. These nanofillers have already been employed to produce a wide range of polymer-based nanocomposites [5, 6], and still more high-modulus polymer nanocomposites are expected to come with a broader application of carbon nanotubes. These hopes appear justified in view of the very high elastic moduli (up to 1000 GPa [9]) of CNTs and theoretical interpretations of nanocomposite properties in the framework of numerous micromechanical models [96]. These models include a relevant parameter of the filler in the calculation of the composite elastic modulus and take account of the relationship between the two characteristics. However, some of the recently proposed models mentioned in Section 3, e.g., percolation [56] and fractal [24] models, disregard the filler elastic modulus. Moreover, micromechanical models also ignore such important (sometimes critical) parameters of polymer composites as the interfacial adhesion level and aggregation degree of initial nanofiller particles. The authors of Refs [160, 161] undertook a theoretical analysis of the prospects for applying the nanofillers considered in the present review to the manufacture of structural polymer nanocomposites for which the reinforcement degree (i.e., the degree of enhancement of the nanocomposite elastic modulus relative to that of the matrix polymer) is the principal measure of efficiency.

In the framework of the modified percolation model, the reinforcement degree of polymer nanocomposites, E_n/E_m, can be described by Eqn (21). To recall, the validity of interpretation of interfacial regions as a reinforcement element in nanocomposites was confirmed in experiments with particulate-filled polymer nanocomposites exemplified by butadiene-styrene rubber/nanoshungite using nanoscopic techniques The elasticity modulus of interfacial regions in these material is only 20% lower than in nanoshungite but six times that in the polymer matrix [162] (see Section 2.4 for details). In this interpretation, the surface structure of nanofiller particles (particle aggregates) is of special importance; it is characterized by fractal dimension d_s determining in fact both the volume fraction of interfacial regions φ_{int} [see Eqn (27)] and the reinforcement degree E_n/E_m [5]:

$$\frac{E_n}{E_m} = 18\left[1 - (d - d_s)^{1/1.7}\right], \tag{93}$$

where d is a dimension of the Euclidean space in which a fractal is considered (clearly, $d = 3$ in our case).

It is easy to see that Eqns (27) and (93) predict an increase in the reinforcement degree with increasing dimension d_s, the value of which can be found theoretically from Eqn (7). Calculation of d_s^{theor} for organoclay (Na$^+$-montmorillonite) using this equation gives 2.77, versus 2.78 observed in experiment [163]. This confirms the adequacy of the proposed method.

However, there is an important aspect of the formation of interfacial layers (or polymer absorption) on fractal surfaces. In the case being considered, the effective quantity d_s (d_s^{eff}) depends on the ability of macromolecules of the matrix polymer to copy ('reproduce') them rather than on the roughness proper of the nanofiller surface. A macromolecule modelled by a sequence of stiff statistical segments ~ 1 nm long 'perceives' the fractal surface having molecular (atomic)-scale roughness as a much smoother one [5], in accordance with the following equation [47]:

$$d_s^{eff} = 5 - d_s^{theor}. \tag{94}$$

Table 3. Characteristics of the main types of polymer nanocomposites [160].

Nanofiller	d_s^{theor}	d_s^{eff}, equation (27)	d_s^{eff}, equation (93)	φ_n^{max}	$(E_n/E_m)^{max}$
Disperse particles	2.60	2.20	2.33	2.33	12.0
Organoclay (exfoliated)	2.78	2.30	2.13	0.246	7.23
Organoclay (intercalated)	2.78	2.15	2.34	0.374	7.21
Carbon nanotubes	2.73	2.27	2.23	0.239	6.76

This relation actually reflects the known dependence of specific surface S_{sp} on the cross section area σ of absorbed molecules [36]:

$$S_{sp} \sim \sigma^{(2-d_s^{eff})/2}. \tag{95}$$

Table 3 presents the values of d_s^{theor} calculated in accordance with Eqn (7), as well as d_s^{eff} values obtained from Eqns (27) and (93). It follows that the relationship between these dimensions is fairly well described by Eqn (94).

Micrometer-size filler particles in a polymer composite are known to build up a spatial backbone structure with dimension D_B ($2 \leqslant D_B \leqslant 3$), which is an analog of the fractal lattice on which the polymer matrix structure forms [24, 26, 164]. This effect results in a change to the matrix structure, characterized by fractal dimension d_f, in comparison with the structure of the matrix polymer. Parameters φ_{int} and D_B are related by Eqn (40).

The relationship between φ_{int} and φ_n for different types of nanofillers can be obtained in the following way. First, the interfacial layer thickness l_{int} is calculated using Eqn (24), then the resulting relation gives Eqn (28), which is reduced to a simpler form [formula (22)] in which coefficient c equals 0.260 for disperse particles with $D_p = 80$ nm, 1.910 and 0.955 for exfoliated and intercalated organoclay, respectively, and 1.86 for CNT [5].

It is known that the dimension of any real fractal cannot be higher than the dimension of the enveloping Euclidean space [165]. Therefore, substituting the quantity $c\varphi_n$ in Eqn (40) for φ_{int} and assuming $D_B = d = 3$ give the estimate of the maximum volumetric filling degree φ_n^{max} for the nanofillers of interest. These φ_n^{max} values are also included in Table 3. The physically unreal value of $\varphi_n^{max} = 2.33$ ($\varphi_n < 1$) for particulate-filled polymer nanocomposites means that condition $D_B = 3$ is unattainable for these materials. Because φ_n^{max} is defined by the condition [5]

$$\varphi_n^{max} = 1 - \varphi_{int} = 1 - 0.26\varphi_n^{max}, \tag{96}$$

it gives $\varphi_n^{max} = 0.794$. Substituting this φ_n^{max} value into Eqn (40) yields the limiting value of $D_B = 1.33$. In other words, disperse nanoparticles in a polymeric matrix cannot form a spatial backbone ($D_B \geqslant 2$) but give rise to more or less branched chains, i.e., they produce an effect well known for elastomer (rubber)-based particulate-filled nanocomposites [72] (see also Section 2.5). Due to chain formation, nanofillers of any type do not change the structure of the matrix polymer, and fractal dimension d_f of the nanocomposite structure is equal to this parameter for the parent matrix polymer [5].

Finally, combining equations (21) and (22) makes it possible to estimate the limiting degree of reinforcement $(E_n/E_m)^{max}$ at $\varphi_n = \varphi_n^{max}$ for the nanofillers of interest. The

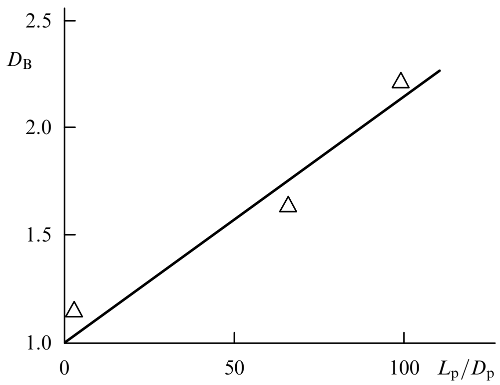

Figure 24. A plot of nanofiller particle backbone dimension D_B vs degree of particle's anisotropy L_p/D_p [160].

estimates of $(E_n/E_m)^{max}$ presented in Table 3 demonstrate that the maximally possible value of $(E_n/E_m)^{max} = 12$ for a composite can be reached only for particulate-filled nanocomposites, because this value for other types of polymer nanocomposites is much lower than 12. Effects realizable under condition of $\varphi_n > \varphi_n^{max}$ can be illustrated most simply by the example of organoclays using a combination of Eqns (40) and (22). Coefficients $c = 1.910$ and 0.955 for exfoliated and intercalated organoclays, respectively, are obtained by the following line of thought [5]. The formation of a 'stack' (tactoid) consisting of two plates of organoclay suggests that only two interfacial layers form on each side of the plate rather than four layers (two on each plate or one on each its side). This means that coefficient $c = 1.910$ decreases twofold in the former case, threefold in the case of a three-plate tactoid, etc. Because the right-hand side of Eqn (40) remains unaltered (at $D_B = 3$), an increase in φ_n on its left-hand side of this equation leads to a decrease in c or (as follows from the above discussion) aggregation of organoclay plates [5].

Let us consider the influence of anisotropy of nanofiller particles on D_B. The level of anisotropy can be defined as the L_p/D_p ratio, where L_p is the particle length, and D_p is the nanofiller particle diameter (or thickness of organoclay). Figure 24 shows the $D_B(L_p/D_p)$ dependence, suggesting a linear increase in D_B with growing the anisotropy level.

To sum up, the application of various methods for nanoparticle dispersion (the use of binding agents [166], mixing components in an electromagnetic field [5], ultrasound [167], etc.) does not change the above estimates, since in any case $D_B \leqslant d$. As soon as D_B exceeds d, nanofiller density begins to increase [i.e., aggregation occurs; see Eqn (15)] because it does not 'fit' into a three-dimensional space [168]. This well-known effect is similar to blood coagulation [169] and globule formation in cross-linked epoxy polymers [120].

6. Conclusion

It has been shown in the foregoing that the fractal dimension of a nanoparticle surface having a strong influence on the formation of the interfacial layer in polymer nanocomposites depends on the ability of polymer macromolecules to 'reproduce' the relief of this surface. The spatial backbone of nanoparticles can form only in anisotropic nanofillers (organoclays and carbon nanotubes). Disperse nanofillers make up chains of particles without alteration of the polymer matrix structure, in contrast to a matrix polymer.

A fundamental difference between percolation and fractal models of the reinforcement of polymer nanocomposites and macromechanical models lies in the fact that the former take no account of the nanofiller elastic modulus. They assume the interfacial regions to be a reinforcement element of the structure, just the same as the nanofiller proper. Each type of nanofiller is characterized by a limiting degree of filling that eventually determines the limiting reinforcement degree of the nanocomposite. Disperse nanofillers are considered to be the most efficacious materials for the production of engineering polymer nanocomposites.

An important factor responsible for the end-use properties of nanocomposites is noticeable aggregation of initial filler particles due to their small sizes and, therefore, large specific surfaces. This effect accounts for a 3–5-fold decrease in the yield stress of a nanocomposite compared with the theoretically attainable value.

The well-known Tabor equation giving a microhardness-to-yield stress ratio equal to 3 holds only for Euclidean solids. The fractality of the polymer matrix structure in a nanocomposite decreases this ratio.

The introduction of a disperse nanofiller into the polymer matrix may substantially improve the thermophysical properties of the nanocomposite being formed. The nanoadhesion effect is responsible for the sharp (several-fold) decrease in the thermal expansion coefficient, whereas the creation of a proper filler structure in the polymer matrix permits enhancing the heat conductivity of nanocomposites. An important technological factor for nanocomposites distinguishing them from microcomposites is constant (or even decreasing) viscosity of the melt in response to a rise in the nanofiller content. This effect can be quantitatively described only in terms of fractal models.

References

1. Poole C P (Jr.), Owens F J *Introduction to Nanotechnology* (Hoboken, NJ: J. Wiley, 2003); Translated into Russian: *Nanotekhnologii* (Moscow: Tekhnosfera, 2004)
2. Sheng N et al. *Polymer* **45** 487 (2004)
3. Malamatov A Kh, Kozlov G V, Mikitaev M A *Mekhanizmy Uprocheniya Polimernykh Nanokompozitov* (Reinforcement Mechanisms of Polymer Nanocomposites) (Moscow: RKhTU, 2006)
4. Mikitaev A, Kozlov G, Zaikov G *Polymer Nanocomposites: Variety of Structural Forms and Applications* (New York: Nova Sci. Publ., 2008); Russian edition: *Polimernye Nanokompozity: Mnogoobrazie Strukturnykh Form i Prilozhenii* (Moscow: Nauka, 2009)
5. Kozlov G V, Yanovskii Yu G , Karnet Yu N *Fiziko-Mekhanicheskie Svoistva Nanostrukturirovannykh Polimernykh Kompozitov v Ramkakh Fraktal'nogo i Mul'tifraktal'nogo Opisaniya* (Physico-Mechanical Properties of Nanostructured Polymer Composites in the Framework of Fractal and Multifractal Descriptions) (Moscow: OneBook, 2013)
6. Kozlov G V, Mikitaev A K *Structure and Properties of Nanocomposites Polymer/Organoclay* (Saarbrücken: LAP Lambert Acad. Publ., 2013)
7. Thostenson E T, Li C, Chou T-W *Composit. Sci. Technol.* **65** 491 (2005)
8. Moniruzzaman M, Winey K I *Macromolecules* **39** 5194 (2006)
9. Eletskii A V *Phys. Usp.* **50** 225 (2007); *Usp. Fiz. Nauk* **177** 233 (2007)
10. Paul D R, Robenson L M *Polymer* **49** 3187 (2008)
11. Okhlopkova A A, Vinogradova A V, Pinchuk L S *Plastiki, Napolnennye Ul'tradispersnymi Neorganicheskimi Soedineniyami* (Plastic Materials Filled with Ultradisperse Inorganic Compounds) (Gomel: Izd. IMMS NANB, 1999)
12. Agag T, Koga T, Takeichi T *Polymer* **42** 3399 (2001)

13. Park J H, Jana S C *Polymer* **44** 2091 (2003)
14. Kotsilkova R (Ed.) *Thermoset Nanocomposites for Engineering Applications* (Shropshire: Smithers Rapra Technology Limited, 2007)
15. Mancini L H, Esposito C L (Eds) *Nanocomposites*: *Preparation, Properties and Performance* (New York: Nova Science Publ., 2008)
16. Šupová M, Martynková G S, Barabaszová K *Sci. Adv. Mater.* **3** 1 (2011)
17. Mittal V (Ed.) *Modeling and Prediction of Polymer Nanocomposite Properties* (Weinheim: Wiley-VCH, 2013)
18. Lipatov Yu S *Mezhfaznye Yavleniya v Polimerakh* (Interfacial Phenomena in Polymers) (Kiev: Naukova Dumka, 1980)
19. Knunyants N N et al. *Mekh. Kompozit. Mater.* **22** 231 (1986)
20. Kozlov G V, Yanovsky Yu G, Lipatov Yu S *Composite Mech. Design* **8** 111 (2001); *Mekh. Kompozits. Mater. Konstruktsii* **8** 111 (2002)
21. Kozlov G V, Yanovsky Yu G, Lipatov Yu S *Composite Mech. Design* **9** 398 (2003); *Mekh. Kompozits. Mater. Konstruktsii* **9** 398 (2003)
22. Afashagova Z Kh et al., in *Materialy Vtorogo Mezhdunarodnogo Mezhdisciplinarnogo Simpoziuma “Fizika Nizkorazmernykh Sistem i Poverkhnostei”* (Proc. of the Second Intern. Interdisciplinary Symp. “Physics of Low-Dimensional Systems and Surfaces”) (Rostov-on-Don: SKNTs VSh YuFU APSN, 2010) p. 122
23. Kozlov G V, Lipatov Yu S *Mekh. Kompozit. Mater.* **40** 827 (2004)
24. Kozlov G V, Yanovskii Yu G , Karnet Yu N *Struktura i Svoistva Dispersno-napolnennykh Polimernykh Kompozitov*: *Fraktal’nyi Analiz* (The Structure and Properties of Particulate-filled Polymer Composites: Fractal Analysis) (Moscow: Al’yanstransatom, 2008)
25. Kozlov G V, Yanovskii Yu G, Zaikov G E *Structure and Properties of Particulate-Filled Polymer Composites*: *the Fractal Analysis* (New York: Nova Science Publ., 2010)
26. Kozlov G V, Yanovsky Yu G, Zaikov G E *Synergetics and Fractal Analysis of Polymer Composites Filled with Short Fibers* (New York: Nova Science Publ., 2011)
27. Kubat J, Rigdahl M, Welander M *J. Appl. Polymer Sci.* **39** 1527 (1990)
28. Kozlov G V, Lipatov Yu S *Vopr. Khim. Khim. Tekhnol.* (3) 65 (2002)
29. Kozlov G V, Lipatov Yu S *Composite Interfaces* **9** 509 (2002)
30. Burya A I, Kozlov G V *Sinergetika i Fraktal’nyi Analiz Polimernykh Kompozitov, Napolnennykh Korotkimi Voloknami* (Synergetics and Fractal Analysis of Polymer Composites Filled with Short Fibers) (Dnepropetrovsk: Porogi, 2008)
31. Malamatov A Kh, Kozlov G V , Mikitaev M A, in *Polikondensatsionnye Reaktsii i Polimery* (Polycondensated Reactions and Polymers) (Nal’chik: KGBU, 2007) p. 134
32. Kozlov G V , Burya A I, Lipatov Yu S *Kompozit. Mater.* (1) 3 (2007)
33. Kozlov G V et al. *Mekh. Kompozits. Mater. Konstruktsii* **13** 479 (2007)
34. Kozlov G V et al., in *Handbook of High- and Low-Molecular Compounds* (Eds R Pethrick, G Zaikov) (New York: Nova Science Publ., 2008) p. 236
35. Burya A I et al. *Mater. Tekhnol. Instrum.* **14** 35 (2009)
36. Holliday L, Robinson J D, in *Polymer Engineering Composites* (Ed. M O W Richardson) (London: Applied Science Publ., 1977) p. 263; Translated into Russian: *Promyshlennye Polimernye Kompozitsionnye Materialy* (Ed. M O W Richardson) (Moscow: Khimiya, 1980) p. 241
37. Tanaka K, Nagamura T, in *Mater. Intern.Conf. on Polymer and Advanced Materials, POLYMEX-2006* Sec. 1 (Mexico: Huatulko, 2006) p. 51
38. Andrievskii R A *Ross. Khim. Zh.* **46** (5) 50 (2002)
39. Wu S *Polymer Interface and Adhesion* (New York: M. Dekker, 1982)
40. Lomakin S M, Zaikov G E *Polymer Sci. B* **47** 9 (2005); *Vysokomolek. Soed. B* **47** 104 (2005)
41. Kozlov G V, Afashagova Z Kh, Burya A I *Nano- Mikrosistem. Tekh.* (3) 45 (2008)
42. Avnir D, Farin D, Pfeifer P *Nature* **308** 261 (1984)
43. Farin D et al. *Langmuir* **1** 399 (1985)
44. Stanley H E et al. *Phys. Rev. Lett.* **53** 1706 (1984)
45. Meakin P et al. *Phys. Rev. A* **32** 2364 (1985)
46. Pfeifer P, Avnir D *J. Chem. Phys.* **79** 3558 (1983)
47. Van Damme H et al. *J. Chem Phys.* **85** 616 (1986)
48. Kozlov G V et al. *Vopr. Khim. Khim. Tekhnol.* (3) 118 (2005)
49. Kozlov G V, Novikov V U, Lipatov Yu S *Materialovedenie* (8) 21 (2000)
50. Kozlov G V, Afashagova Z Kh, Zaikov G E *Khim. Fiz. Mezoskop.* **10** 181 (2008)
51. Kozlov G V, Afashagova Z Kh, Zaikov G E *Vestn. MITKhT* **4** (3) 89 (2009)
52. Yakubov T S *Dokl. Akad. Nauk SSSR* **303** 425 (1988)
53. Kozlov G V et al., in *Materialy 8-go Mezhdunarodnogo Simpoziuma “Poryadok, Besporyadok i Svoistva Oksidov”, Sochi, 2005* (Proc. of the 8th Intern. Symp. “Order, Disorder and Properties of Oxides,” Sochi 2005), p. 208
54. Kozlov G V, Burya A I, Lipatov Yu S, in *II Mezhdunar. Nauch.-Tekhn. Konf. “Analiticheskie i Chislennye Metody Modelirovaniya Estestvennonauchnykh i Sotsial’nykh Problem”* (II Intern. Science and Technology Conf. “Analytical and Numerical Methods for Modeling Natural and Social Problems”) (Penza: PGU, 2007) p. 79
55. Kozlov G V et al. *Mekh. Kompozits. Mater. Konstruktsii* **12** 99 (2006)
56. Bobryshev A N et al. *Sinergetika Kompozitnykh Materialov* (Synergetics of Composite Materials) (Lipetsk: NPO ORIUS, 1994)
57. Dickie R A, in *Polymer Blends* Vol. 1 (Eds D R Paul, S Newman) (New York: Academic Press, 1978) p. 353; Translated into Russian: *Polimernye Smesi* Vol. 1 (Eds D R Paul, S Newman) (Moscow: Mir, 1978) p. 397
58. Kozlov G V et al. *Dopovidi Nats. Akad. Nauk Ukraïni* (7) 148 (2006)
59. Kozlov G V et al. *Nanotekhnika* (1) 81 (2008)
60. Mikitaev A K et al. *Plasticheskie Massy* (12) 45 (2004)
61. Lazorenko M V et al. *Kauchuk Rezina* (1) 17 (1988)
62. Kozlov G V, Yanovskii Yu G, Zaikov G E, in *Polymer Yearbook-2011. Polymers, Composites and Nanocomposites* (Eds G Zaikov, C Sirghie, R Kozlowski) (New York: Nova Science Publ., 2011) p. 218
63. Korneev Yu V et al. *Kauchuk Rezina* (6) 18 (2008)
64. Hentschel H G E, Deutch J M *Phys. Rev. A* **29** 1609(R) (1984)
65. Kozlov G V, Novikov V U *Phys. Usp.* **44** 681 (2001); *Usp. Fiz. Nauk* **171** 717 (2001)
66. Wu S *J. Polymer Sci. B* **27** 723 (1989)
67. Aharoni S M *Macromolecules* **16** 1722 (1983)
68. Budtov V P *Fizicheskaya Khimiya Rastvorov Polimerov* (Physical Chemistry of Polymer Solutions) (St. Petersburg: Khimiya, 1992)
69. Kozlov G V, Yanovskii Yu G, Karnet Yu N *Mekh. Kompozits. Mater. Konstruktsii* **11** 446 (2005)
70. Novikov V U, Kozlov G V, Bur’yan O Yu *Mekh. Kompozit. Mater.* **36** 3 (2000)
71. Lipatov Yu S *Physical Chemistry of Filled Polymers* (Shrewsbury: Rubber and Plastics Res. Associat. of Great Britain, 1979); Translated from Russian: *Fizicheskaya Khimiya Napolnennykh Polimerov* (Moscow: Khimiya, 1977)
72. Bartenev G M, Zelenev Yu V *Fizika i Mekhanika Polimerov* (Polymer Physics and Mechanics) (Moscow: Vysshaya Shkola, 1983)
73. Kozlov G V, Mikitaev A K *Mekh. Kompozits. Mater. Konstruktsii* **2** 144 (1996)
74. Kozlov G V, Yanovskii Yu G, Mikitaev A K *Mekh. Kompozit. Mater.* **34** 539 (1998)
75. Balankin A S *Sinergetika Deformiruemogo Tela* (Synergetics of Strained Body) (Moscow: Izd. Ministerstva Oborony SSSR, 1991)
76. Hornbogen E *Int. Mater. Rev.* **34** 277 (1989)
77. Pfeifer P *Appl. Surf. Sci.* **18** 146 (1984)
78. Avnir D, Farin D, Pfeifer P *J. Colloid Interface Sci.* **103** 112 (1985)
79. Kozlov G V, Mikitaev A K *Nanotekhnol. Nauka Proizvodstvo* (4) 57 (2011)
80. Ishikawa K *J. Mater. Sci. Lett.* **9** 400 (1990)
81. Ivanova V S et al. *Sinergetika i Fraktaly v Materialovedenii* (Synergetics and Fractals in Materials Science) (Moscow: Nauka, 1994)
82. Vstovskii G V, Kolmakov L G, Terent’ev V F *Metally* (4) 164 (1993)
83. Hansen J P, Skjeitorp A T *Phys. Rev. B* **38** 2635 (1988)
84. Pfeifer P, Avnir D, Farin D *J. Stat. Phys.* **36** 699 (1984)
85. Osman A M, Atallah A, Suter U W *Polymer* **45** 1177 (2004)
86. Xie X-L et al. *Polymer* **45** 6665 (2004)
87. Yang K et al. *Mater. Lett.* **60** 805 (2006)

88. Kozlov G V et al. *Mekh. Kompozits. Mater. Konstruktsii* **15** 137 (2009)
89. Kozlov V G et al. *Naukoemkie Tekhnol.* **12** (3) 17 (2011)
90. Tugov I I, Shaulov A Yu *Vysokomolek. Soed. B* **32** 527 (1990)
91. Sumita M et al. *J. Mater. Sci.* **18** 1758 (1983)
92. Honeycombe R W K *The Plastic Deformation of Metals* (London: Edward Arnold, 1968); Translated into Russian: *Plasticheskaya Deformatsiya Metallov* (Moscow: Mir, 1972)
93. Kozlov V G, Sanditov D S *Angarmonicheskie Effekty i Fiziko-mekhanicheskie Svoistva Polimerov* (Anharmonic Effects and Physicomechanical Properties of Polymers) (Novosibirsk: Nauka, 1994)
94. Kozlov V G, Ovcharenko E N, Mikitaev A K *Struktura Amorfnogo Sostoyaniya Polimerov* (The Structure of Amorphous Polymers) (Moscow: Izd. RKhTU im. D I Mendeleeva, 2009)
95. Piggott M R, Leidner J *J. Appl. Polymer. Sci.* **18** 1619 (1974)
96. Ahmed S, Jones F R *J. Mater. Sci.* **25** 4933 (1990)
97. Edwards D C *J. Mater. Sci.* **25** 4175 (1990)
98. Afashagova Z Kh et al. *Materialovedenie* (9) 10 (2007)
99. Kozlov G V, Grineva L G, in *IX Mezhdunar. Nauchn.-Tekhn. Konf. "Materialy i Tekhnologii XXI Veka"* (IXth Intern. Scientific and Technical Conf. "Materials and Technologies of XXI Century") (Penza: PGU, 2011) p. 12
100. Counto U J *Mag. Concr. Res.* **16** 129 (1964)
101. Kozlov G V, Shoranova L O, Mikitaev A K, in *VI Mezhdunar. Nauchn.-Tekhn. Konf. "Problemy Issledovaniya i Proektirovaniya Mashin"* (VIth Intern. Scientific and Technical Conf. "Problems of Research and Design of Machines") (Penza: PGU, 2010) p. 96
102. Kalinchev E L, Sakovtseva M B *Svoistva i Pererabotka Termoplastov* (Properties and Processing of Thermoplasts) (Leningrad: Khimiya, 1983)
103. Wu S-H et al. *Mater. Lett.* **49** 327 (2001)
104. Sultonov N Zh, Mikitaev A K, in *Materialy VI Mezhdunar. Nauchn.-Tekhn. Konf. "Novye Polimernye Kompozitsionnye Materialy"* (Proc. of the 6th Intern. Scientific and Technical Conf. "New Polymeric Composite Materials") (Nal'chik: KBGU, 2010) p. 392
105. Bashorov M T, Kozlov G V, Mikitaev A K *Nanostruktury i Svoistva Amorfnykh Stekloobraznykh Polimerov* (Nanostructures and Properties of Amorphous Glassy Polymers) (Moscow: Izd. RKhTU im. D I Mendeleeva, 2010)
106. Kozlov G V, Mikitaev A K *Polymers as Natural Nanocomposites: Unrealized Potential* (Saarbrücken: Lambert Acad. Publ., 2011)
107. Kozlov G V et al. *Izv. Kabardino-Balkarskogo Gos. Univ.* (4) 443 (2011)
108. Aharoni S M *Macromolecules* **18** 2624 (1985)
109. Magomedov G M, Kozlov G V *Sintez, Struktura i Svoistva Polimerov i Nanokompozitov na Ikh Osnove* (Synthesis, Structure and Properties of Polymers and Polymer-Based Nanocomposites) (Moscow: Akademiya Estestvoznaniya, 2010)
110. Magomedov G M, Kozlov G V, Zaikov G E *Structure and Properties of Cross-Linked Polymers* (Shawbury: Smithers Group Co., 2011)
111. Bashorov M T et al., in *Handbook of Condensed Phase Chemistry* (Eds G Zaikov, V Kablov) (New York: Nova Science Publ., 2010) p. 33
112. Family F *J. Stat. Phys.* **36** 881 (1984)
113. Kozlov G V et al. *Tech. Phys. Lett.* **22** 657 (1996); *Pis'ma Zh. Tekh. Fiz.* **22** (16) 31 (1966)
114. Narisawa I *Prochnost' Polimernykh Materialov* (The Strength of Polymer Materials) (Moscow: Khimiya, 1987)
115. Brown N *Mater. Sci. Eng.* **8** 69 (1971)
116. Kozlov G V et al. *Naukoemkie Tekhnol.* (12) 32 (2011)
117. Balankin A S, Bugrimov A L *Vysokomolek. Soed. A* **34** 135 (1992)
118. Balankin A S et al. *Dokl. Akad. Nauk SSSR* **326** 463 (1992)
119. Leidner J, Woodhams R T *J. Appl. Polymer Sci.* **18** 1639 (1974)
120. Phillips D, Harris B, in *Polymer Engineering Composites* (Ed. M O W Richardson) (London: Applied Science Publ., 1977) p. 45; Translated into Russian: *Promyshlennye Polimernye Kompozitsionnye Materialy* (Ed. M O W Richardson) (Moscow: Khimiya, 1980) p. 50
121. Tanniru M, Misra R D K *Mater. Sci. Eng. A* **405** 178 (2005)
122. Kozlov G V *Nanotekhnika* (2) 33 (2008)
123. Zaikov G E et al. *J. Appl. Polymer Sci.* **111** 2621 (2009)
124. Afashagova Z Kh, Kozlov G V, Malamatov A Kh *Mezhdunar. Zh. Priklad. Fundament. Issled.* (3) 38 (2009)
125. Koslov G V, Serdyuk V D, Dolbin I V *Materialovedenie* (12) 2 (2000)
126. Deshmane C, Yuan Q, Misra R D K *Mater. Sci. Eng. A* **452–453** 592 (2007)
127. Bucknall C B *Toughened Plastics* (London: Applied Science Publ., 1977); Translated into Russian: *Udaroprochnye Plastiki* (Leningrad: Khimiya, 1990)
128. Bartenev G M, Frenkel' S Ya *Fizika Polimerov* (Polymer Physics) (Leningrad: Khimiya, 1990)
129. Kozlov G V, Misra R D K, Afashagova Z Kh *Nanotekhnika* (2) 71 (2009)
130. Kozlov G V et al. *Chem. Chem. Technol.* **5** 289 (2011)
131. Kuzeev I R et al. *Slozhnye Sistemy v Prirode i Tekhnike* (Complex Systems in Nature and Technique) (Ufa: Izd. UGNTU, 1997)
132. Kausch H H *Polymer Fracture* (Berlin: Springer-Verlag, 1978); Translated into Russian: *Razrushenie Polimerov* (Moscow: Mir, 1981)
133. Afashagova Z Kh et al., in *Mater. Khar'kovskoi Nanotekhnologicheskoi Assamblei* (Proc. of the Kharkov Nanotechnological Assembly) (Khar'kov: KhGU, 2007) p. 204
134. Kozlov G V, Zaikov G E, in *Fractals and Local Order in Polymeric Materials* (Eds G Kozlov, G Zaikov) (New York: Nova Science Publ., 2001) p. 55
135. Balta-Calleja F J, Kilian H G *Colloid Polymer Sci.* **266** 29 (1988)
136. Balta-Calleja F J et al. *Colloid Polymer Sci.* **268** 440 (1990)
137. Aloev V Z, Kozlov G V *Fizika Orientatsionnykh Yavlenii v Polimernykh Materialakh* (Physics of Orientation Phenomena in Polymer Materials) (Nal'chik: Poligrafservis i T, 2002)
138. Perry A J, Rowcliffe L J *J. Mater. Sci. Lett.* **8** 904 (1973)
139. Sanditov D S, Bartenev G M *Fizicheskie Svoistva Neuporyadochennykh Struktur* (Physical Properties of Disordered Structures) (Novosibirsk: Nauka, 1982)
140. Kohlstedt D L *J. Mater. Sci.* **8** 777 (1973)
141. Kozlov G V et al. *Fiz.-Khim. Mekh. Mater.* **36** 98 (2000)
142. Afashagova Z Kh et al. *Kompozit. Mater.* (3) 22 (2009)
143. Suwanprateeb J *Composites A* **31** 353 (2000)
144. Zebarjiad S M, Sajjadi S A *Mater. Sci. Eng. A* **475** 365 (2008)
145. Tabor D *The Hardness of Metals* (New York: Oxford Univ. Press, 1951)
146. Afashagova Z Kh et al. *Theor. Found. Chem. Eng.* **41** 896 (2007); *Teor. Osnovy Khim. Tekhnol.* **41** 699 (2007)
147. Aphashagova Z Kh et al. *J. Balkan Tribologic Assoc.* **13** 367 (2007)
148. Kozlov G V et al. *Perspektivnye Mater.* (3) 65 (2009)
149. Maxwell D, Young R J, Kinloch A J *J. Mater. Sci. Lett.* **3** 9 (1984
150. Stanley H, in *Fractals in Physics* (Eds L Pietronero, E Tosatti) (Amsterdam: North-Holland, 1986); Translated into Russian: *Fraktaly v Fizike* (Eds L Pietronero, E Tosatti) (Moscow: Mir, 1988) p. 463
151. Zeebland H, in *Polymer Engineering Composites* (Ed. M O W Richardson) (London: Applied Science Publ., 1977); Translated into Russian: *Promyshlennye Polimernye Kompozitsionnye Materialy* (Ed. M O W Richardson) (Moscow: Khimiya, 1980) p. 284
152. Kolzov G V, Burya A I, Dolbin I V *J. Eng. Thermophys.* **13** 129 (2005)
153. Kolzov G V et al. *J. Appl. Polymer Sci.* **100** 3828 (2006)
154. Tovmasyan Yu M, Topolkaraev V A, Berlin Al Al *Vysokomolek. Soed. A* **28** 1162 (1986)
155. Burya A I, Chigvintseva O P, Suchilina-Sokolenko S P *Poliakrilaty: Sintez, Svoistva, Kompozitsionnye Materialy* (Polyacrylates: Synthesis, Properties, Composite Materials) (Dnepropetrovsk: Nauka i Prosveshchenie, 2001)
156. Kolzov G V, Tlenkopachev M A, Zaikov G E, in *Abstracts of 11th Internat. Conf. on Frontiers of Polymers and Advanced Materials* (Pretoria, South Africa, 2011) p. 161
157. Kolzov G V et al., in *Unique Properties of Polymers and Composites: Pure and Applied Science* (Eds Yu Bubnov et al.) (New York: Nova Science Publ., 2011) p. 268
158. Mills N J *J. Appl. Polymer Sci.* **15** 2791 (1971)
159. Gol'dshtein R V, Mosolov A B *Dokl. Ross. Akad. Nauk* **324** 576 (1992)

160. Kozlov G V, Zhirikova Z M, Aloev V Z *Nanotekhnol. Nauka Proizvodstvo* (4) 87 (2011)
161. Kolzov G V, Zaikov G E *J. Characteriz. Develop. Novel Mater.* **2** 13 (2010)
162. Kolzov G V, Yanovskii Yu G, Zaikov G E *Chem. Chem. Technol.* **5** 289 (2011)
163. Pernyeszi T, Dekany I *Colloid Polymer Sci.* **281** 73 (2003)
164. Mikitaev A K, Kozlov G V *Fraktal'naya Mekhanika Polimernykh Materialov* (Fractal Mechanics of Polymer Materials) (Nal'chik: Izd. KBGU, 2008)
165. Feder J *Fractals* (New York: Plenum Press, 1988); Translated into Russian: *Fraktaly* (Moscow: Mir, 1991)
166. Khaboshesku V N, Barrera E V, Lobo R F M *Current Res. Nanotechnol.* **1** 165 (2007)
167. Ryabenko A G, in *Proc. of Intern. Conf. "Deformation and Fracture of Materials and Nanomaterials", Moscow, 2007*, p. 411
168. Balankin A S et al. *Sov. Tech. Phys. Lett.* **17** 504 (1991); *Pis'ma Zh. Tekh. Fiz.* **17** (14) 27 (1991)
169. Grosberg A Yu, Khokhlov A R *Fizika v Mire Polimerov* (Physics in the World of Polymers) (Moscow: Nauka, 1989)
170. Kozlov G V et al. *Voprosy Khim. Khim. Tekhnol.* (6) 77 (2002)